PREDICTION OF MECHANICAL PROPERTIES OF CREASES IN THIN FOLDED MEMBRANES

Seyon Mierunalan

178038C

Degree of Master of Science

Department of Civil Engineering

University of Moratuwa
Sri Lanka

July 2018

PREDICTION OF MECHANICAL PROPERTIES OF CREASES IN THIN FOLDED MEMBRANES

Seyon Mierunalan

178038C

Thesis submitted in partial fulfilment of the requirements for the degree of Master of Science in Civil Engineering

Department of Civil Engineering

University of Moratuwa
Sri Lanka

July 2018

Declaration

I declare that this is my own work and this thesis does not incorporate without acknowledgement any material previously submitted for a Degree or Diploma in any other University or institute of higher learning and to the best of my knowledge and belief it does not contain any material previously published or written by another person except where the acknowledgement is made in the text.

Also, I hereby grant to University of Moratuwa the non-exclusive right to reproduce and distribute my thesis, in whole or in part in print, electronic or other medium. I retain the right to use this content in whole or part in future works (such as articles or books).

..... Date :

S.Mierunalan

The above candidate has carried out research for the Masters thesis under my supervision.

..... Date :

Dr. H.M.Y.C. Mallikarachchi

Abstract

Thin membranes underpin many light weight deployable space systems. Folds introduced in these membrane structures for logistics and storage, alter their in-orbit behaviour while deploying. Numerical modelling is relied on as a promising tool in studying the deployment behaviour of these space structures. However, most numerical models aimed at studying deployment behaviour, fail to incorporate fold-line properties due to unavailability of reliable experimental data.

In this research, an attempt has been made to virtually predict the fold-line mechanics using finite element analysis. For this purpose, materially and geometrically nonlinear contact analyses using Abaqus FEA were performed to simulate creased geometry and conduct numerical tensile tests on single folded thin Kapton membranes. Moment - angle responses were plotted using results of simulations and compared with the data obtained from physical experiments and a justifiable agreement was achieved. A further comparison with results from Elastica theory highlights the viability of the proposed numerical approach over analytical models. The use of virtual simulations to characterize the mechanics of fold-lines has proved to be an efficient technique.

The developed fold-line behaviour model was then implemented in commercial finite element package, Abaqus for deployment simulation of single folded thin Kapton membranes using connector elements defined with rotational stiffness. The results were validated against physical experiments and compared with other simulation techniques found in literature. The proposed technique with connector elements is meritorious over other techniques as it captures both the deformed profile and axial displacements along the folded membrane with close agreement with experimental results.

A quasi-static deployment simulation of a solar sail model with thin membrane wrapped around a polygonal hub was carried out using Abaqus/Explicit package to study the deployment behaviour. The fold-line idealisation scheme with connectors defined with rotational stiffness was used to model the fold-lines in this multiply-creased membranes. However, the fold-line stiffness had little effect on the deployment force of the sail in the range of deployment carried out experimentally .

Keywords : *ultra-thin membranes, finite element simulations, fold-line mechanics, rotational stiffness, neutral angle*

Dedication

To my parents and brother, without whom none of this would be possible.

Acknowledgement

First and foremost, I would like to thank my supervisor Dr. Chinthaka Mallikarachchi, for his technical guidance and valuable insights throughout the past year. Without his support, this would have not been possible. I would also like to express my gratitude for the valuable comments and advice given by Prof. Priyan Dias and Prof. Rangika Halwatura during progress reviews.

Next, my gratitude goes to the academic staff members of Department of Civil Engineering of University of Moratuwa. My sincere appreciation to Chamith Deemantha, Milinda Yapa, Varakini Sanmugadas, Sahangi Dassanayake, Hasitha Wijesuriya and Hasini Weerasinghe for being great research colleagues and for their support and helpful conversations throughout my research work. I am grateful to everyone who helped in any way possible to make this a success.

Finally, I would like to thank Ministry of Science, Technology and Research under Indo - Sri Lanka Joint Research Project, National Research Council, Sri Lanka and Senate Research Committee of University of Moratuwa for the financial assistance provided.

Contents

List of Figures

List of Tables

Nomenclature

List of Abbreviations

DLR German Aerospace Centre (Deutsches Zentrum fr Luft- und Raumfahrt)

ESA European Space Agency

IKAROS Interplanetary Kite-craft Accelerated by Radiation of the Sun

JAXA Japanese Aerospace Exploration Agency

LEO Low Earth Orbit

NASA National Aeronautics and Space Administration

List of Symbols

α Time scaling factor

β Connector constitutive rotation

β_i Connector initial angular position

Δt Minimum stable time increment

ϵ_{nom} Nominal strain

ϵ_{pla} Plastic strain

ϵ_{tru} True strain

$\hat{V_i^j}$ Vector in the i^{th} direction for node j

μ_0 Contact damping coefficient

ν Poisson's ratio

ω_{max}	Highest Eigen value of the model
ϕ	Neutral angle
ρ	Material density
σ_{nom}	Nominal stress
σ_{nom}	True stress
θ	Current fold opening angle
ξ	Fraction of critical damping in the fundamental frequency mode
A	Nodal area
c_d	Dilatational wave speed
c_v	Viscous damping coefficient
D	Current sail diameter
d	Creasing gauge between parallel plates
D_f	Fully deployed diameter of the sail
dt	Assigned stable time increment
E	Modulus of elasticity
e	External load vector
E_i	Internal energy of the system (elastic, inelastic and artificial strain energy
E_{ke}	Kinetic energy
E_{total}	Total energy of the system
E_{vd}	Energy absorbed by viscous dissipation
E_{wk}	Work of external forces
F	Tensile load
f	Mass scaling factor
f_{vd}	Contact damping force for penalty contact
I	Second moment of area
i	Internal load vector
j	Number of radial tabs

k	Fold-line stiffness
k_o	Fold-line stiffness during angle opening
k_r	Fold-line stiffness during relaxation
l	Length of the half membrane coupon
L^*	Non-dimensional length
l_h	Distance from the fold-line to the loaded tip
l_{min}	Shortest length of the finite element
M	Resistive moment at the fold-line
m	Mass matrix
M_c	Kinematic moment in the connector
M_i	Bending moment in the i^{th} direction
N	Number of sides of the polygonal hub
n	Normal vector
p	Viscous pressure
P_i^j	Coordinates of j^{th} vertex in i^{th} fold-line
q	Deployment rate
R	Radius of the circumcircle of the polygonal hub
r_i	Rotation about the i^{th} axis
t	Thickness
u	Spacing between adjacent layers in the folded configuration
u_i	Displacement in the i^{th} direction
v	Velocity
v_{rel}^{el}	Rate of relative motion between two surfaces
w	Width of the membrane coupon
z_j	z coordinate of j^{th} vertex

Chapter 1

Introduction

1.1 Deployable Membrane Structures

Deployable sunshields, inflatable telescopes, solar arrays and solar sails are some deployable space structures constructed with thin membranes [1, 2, 3]. Engineers leverage the two dimensional nature of thin membranes for these space applications requiring large surface area for in-space operation, tens to hundreds of metres [4], but low areal density while in-flight [5]. In general, a large area is required for two reasons: 1) to increase the quantity of flux collected (solar radiation in the case of solar sails) and 2) to achieve high aperture, thus high spatial resolution of signals transmitted from space. Figure 1.1 shows an artist's concept of LightSail spacecraft by the Planetary Society to demonstrate solar sail propulsion.

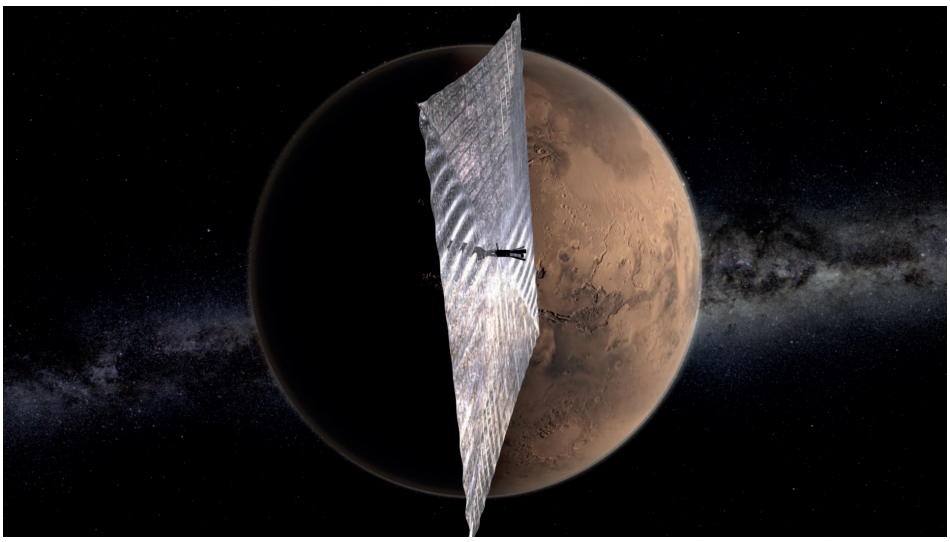

Figure 1.1: Artist′s concept of LightSail spacecraft near Mars (courtesy: The Planetary Society)

Packaging into the limited storage space of launch vehicles and reliable tear-free deployment for operation after launching into space create fundamental challenges in design of these structures. Out of which prediction of deployment behaviour is the most difficult without conducting flight tests.

1.2 State of the Art

In 2001, a 20 m square solar sail divided into four right-triangular quadrants was tested in vacuum, sponsored by NASA [6]. The sail was deployed by four booms. Hence the independent behaviour of sail membrane could not be quantified. The primary objective was to characterize the behaviour of the deployed sail craft rather than studying the deployment mechanics of the sail membrane. The difficulty in testing under representative space environment was also highlighted.

JAXA during its IKAROS mission conducted experimental studies to characterize centrifugal sail deployment [7]. But the experiments were dynamic that had inertia playing a dominant role. Figure 1.2 illustrates the centrifugal deployment process of IKAROS.

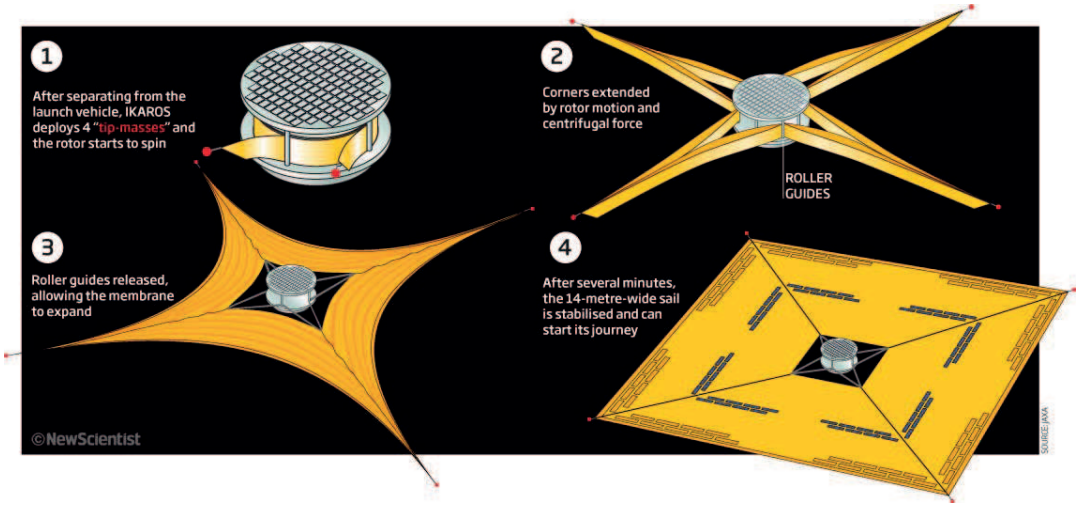

Figure 1.2: Centrifugal deployment process of IKAROS (courtesy: JAXA)

DLR and ESA conducted experiments with 5m x 5m square sail made of 7.5 μm thick aluminized Kapton [8]. The deployment forces were measured but

(a) Folded state

(a) Deployed state

Figure 1.3: Ground testing of NanoSail-D2 using a low friction table (courtesy: NASA)

(a)

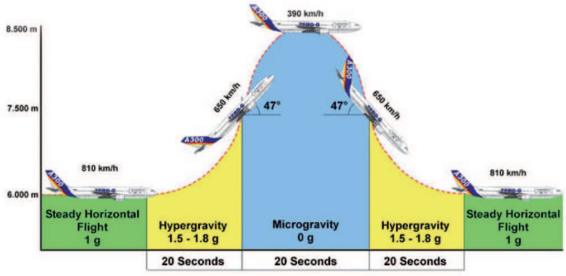

(b)

Figure 1.4: Parabolic flight
(a) Airbus A300 in parabolic flight (b) maneuver cycle (courtesy: ESA)

were influenced by gravity and air drag since it was done at higher deployment rates (25 mm/s approx.).

NanoSail-D2 of NASA demonstrated a 3.14 m x 3.14 m sail of 2.5 μm-thick CP1 deployed in Low Earth Orbit (LEO) from a 3U CubeSat [9]. The sail was divided into four right-triangular quadrants with four deployable booms. Low friction tables were used to offload gravity in ground deployment tests as shown in Figure 1.3. However, with shorter time frame, the deployment mechanism of the sail membrane was not characterized.

In 2015, the Planetary Society's LightSail-1 packaged 32 m^2 Mylar solar sail in a 3U CubeSat [10]. The mission suffered atmospheric drag since the altitude was too low. LightSail-2, currently under development to demonstrate controlled solar sailing is planned to be deployed at a higher altitude [11]. Both

missions utilized low friction tables for initial deployment tests.

The above missions highlight gravity and air drag as two variables that are present in testing deployable membrane structures in Earth but are not present in space. Gravity offload systems are widely used to eliminate gravity, but they are more applicable to sufficiently stiff structures whose deployment is motorized. Less stiff nature of membranes which have thickness in the order of micrometres, causes them to sag which can change the deployment mechanics significantly.

Drop towers and zero-gravity flights (see Figure 1.4) are two other options. These approaches are acceptable for small structures with seconds of deployment time and are either rugged enough to survive the fall or inexpensive enough to replace after each test. However, air drag is still present. This can be problematic while deploying. Conducting experiments in a vacuum chamber is an option to eliminate air drag, but it can be costly and time consuming.

1.3 Testing in Virtual Environments

The time consuming and costly nature of physical testing of membrane structures call for an alternative that can be used in design optimization of these structures that may require several design cycles. There are two approaches followed in this regard.

The first approach is to employ analytical methods to study the behviour of these folded membrane structures. Filipov et al. [12] have developed a bar and hinge model that can capture stretching and shearing of the membranes, bending of the membranes and bending along fold-lines. Funase et al. [13] have developed a spring-mass model where membrane is assumed to be isotropic and substituted by particles connected by springs and dampers. However these approaches fail to capture contact and discontinuities like dynamic snapping (a significant change of geometry of the structure within a very small time interval) which are significant factors in the study of deployment of the membrane structures.

The second approach is to employ numerical models to study the behaviour of these folded membrane structures. The present commercial finite element

packages have robust algorithms to capture contact and the discontinuities involved. This makes this approach more viable compared to pure analytical approach. However, it is important to have accurate idealisation schemes in the virtual models to realize accuracy with low computational cost.

For simplicity, most of these simulations have neglected the effects arising from membrane folding, i.e. it is often found that the most virtual simulations idealise the fold or crease lines as perfect hinges. The initial failure of IKAROS demonstrator mission by JAXA [14] has highlighted this shortcoming. This has led engineers to review the techniques to incorporate fold-line mechanics in virtual models [15, 16]. However, the implementation is limited due to unavailability of reliable fold-line behaviour data, as experimental studies in this regard are bottle-necked by measurement challenges.

1.4 Scope and Aim

The broad aim of this research is to develop constitutive fold-line behaviour models of thin membranes through virtual simulations. Simulation is required to overcome the measurement challenges associated with physical experiments that make the determination of these key properties cost prohibitive. The developed model can be fed into the simulation technique proposed by [16] to study the deployment behaviour of thin-folded membrane structures. This will lead to a better understanding of these structures and realization of efficient designs.

Kapton polyimide membranes are considered in this study. Kapton can maintain excellent physical, electrical and mechanical properties over a wide range of temperatures (-269° C to 400° C) [17]. Such durability properties makes it ideal for space applications.

First, materially and geometrically nonlinear contact analyses using commercial finite element package Abaqus/Standard [18] were performed to simulate folded geometry and conduct numerical tensile tests on single folded thin Kapton membranes. Moment−angle responses were plotted using results of simulations and validated with experiments carried out by Dharmadasa et al. [19]. The possibility of quantifying fold-line mechanics using an analytical model based on Elastica theory was explored.

The developed fold-line behaviour model was then implemented in finite element deployment simulation of single folded thin Kapton membranes using simulation technique presented in [16] and compared with simulation techniques presented in [15, 20]. A quasi static deployment simulation of a solar sail model based on the crease pattern proposed by Guest and Pellegrino [21] was carried out using Abaqus/Explicit package to study the deployment behaviour.

1.5 Chapter Organisation

This thesis consists of six chapters. After the current introductory chapter, Chapter 2 gives an overview of literature on creased membranes and past study on characterising their behaviour experimentally and numerically. Specific focus is given to the study on fold-lines and a review of how fold-lines are idealised in existing simulations is also presented.

Chapter 3 focuses on predicting mechanical properties of fold-lines of single folded thin membranes using numerical simulations. The fold-line mechanics is explained first, followed by a simulation technique to predict the mechanical properties involved. The possibility of quantifying fold-line mechanics using an analytical model based on Elastica theory is also explored.

Chapter 4 describes how the predicted mechanical properties in Chapter 3 are to be incorporated in finite element packages. For demonstration, unfolding of a single folded Kapton membrane to an external tensile load is simulated using commercial finite element package Abaqus/Standard and validated against physical experiments. A comparison with existing simulation techniques from literature is also presented.

Chapter 5 presents a quasi-static simulation technique to study the deployment behaviour of a solar sail with the proposed fold-line idealisation technique presented in Chapter 4. A brief introduction to the available features, simulation parameters and necessary checks is presented. The sensitivity of the simulation to various parameters is investigated.

Chapter 6 concludes the thesis with suggestions for future research.

Chapter 2

Literature Review

This chapter provides an overview of literature on creased membranes, their applications and past study on characterizing their behaviour experimentally and numerically. The chapter begins with an introduction to tessellated membranes, various crease patterns that are utilized to form these tessellations and their applications. Next a review of study on fold-lines that cause change in behaviour of these tessellated membranes is presented. The final section gives an overview of existing numerical modelling techniques to characterise the behaviour of these tessellated membranes.

2.1 Tessellated Membranes

A fold in a membrane can be categorized into two, viz; elastic, recoverable and non localized deformation, *bend* and plastic, permanent and localized deformation, *crease*. Creases or fold-lines are formed by scoring or folding thin membranes, thereby adding permanent ridges to the membranes, which are known to enhance directional stiffness whilst promoting flexibility in other directions. Systematic creasing of membranes creates tessellated membranes which engineers make use of to develop numerous applications.

2.1.1 Crease patterns

Traditionally, the Japanese art of Origami has been employed in developing tessellated membranes to achieve the high compaction and required alteration of material properties. The design of crease patterns being the core of this tessellated membranes, several designs have been formulated.

One such pattern to achieve biaxial compaction was developed by Miura [22] as shown in Figure 2.1. Miura-ori pattern where the fold-lines are aligned at a

specific angle allowing a large sheet to be easily folded with a simple linear motion. The presence of plastic deformations, i.e. creases is found to be influential in material state and mechanical response of these highly compacted thin membranes, for instance, unusual response to stretching and bending and negative Poisson's ratio [23] as illustrated in Figure 2.1(b,c and d). Filipov et al. [24] used Miura-ori pattern to create origami tubes that can be reconfigured into numerous geometries.

Guest [21] proposed a mathematical relationship to derive a wrapping pattern based on the polygonal shape. This pattern allows a single membrane to be wrapped around the central hub which will provide a higher stability in deployed state, compared to a membrane made by attaching small portions (see Figure 2.2(c).

Other examples are the tessellations obtained when tiling the plane with a six-crease waterbomb base which has been used to create an origami stent (see Figure 2.2(b)) [26]. Tesellation developed by Ron Resch [25] as illustrated in Figure 2.2(a) has inspired scientists to create origami-based mechanical metamaterials [27].

2.1.2 Applications

Tessellated membranes are widely used in deployable structures. Deployable structures are structures that can be reduced in size for storage and transportation. Folding is the simplest of solutions for achieving the compaction requirement for transportation of large planar structures Section 1.1 describes the application of this concept in space.

However, this concept has been employed in numerous other applications. For one, automotive designers have been developing airbags that can achieve high compaction and rapid deployment using this concept [29]. NASA′s novel concept for a cooling radiator consists of Miura-Ori configuration allowing the radiator to expand or contract depending on the external temperature [30].

Another application of tessellated membranes is reconfigurable meta-materials. Tessellations in micron scale enable materials to achieve properties such as stiffness and strength that are not present inherently. Other

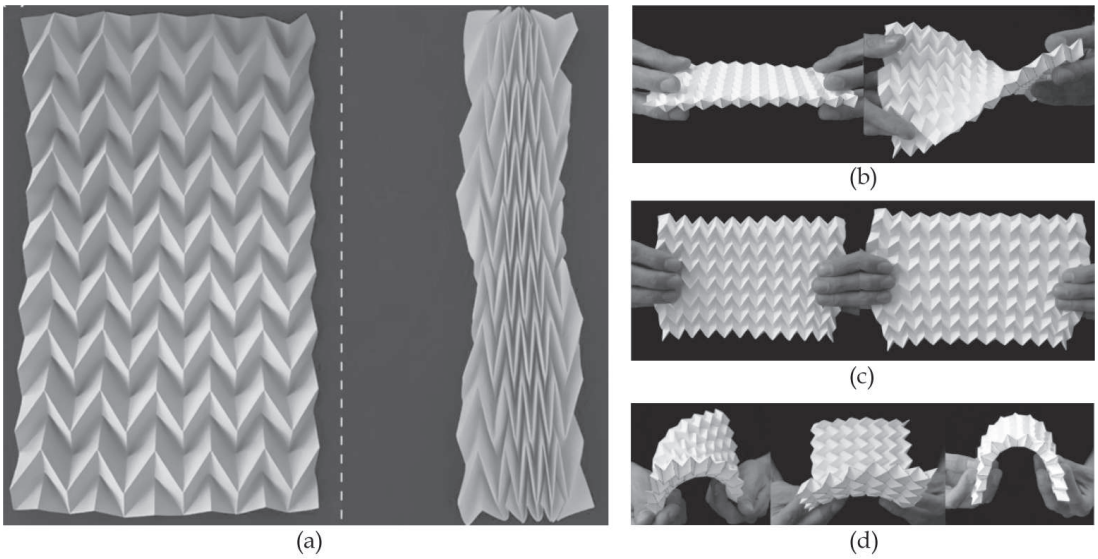

Figure 2.1: Behaviour of Miura-ori described in [23]
(a)tessellation pattern, (b) negative Gaussian curvature response to twisting, (c) negative Poisson's ratio response to stretching and (d) response to bending

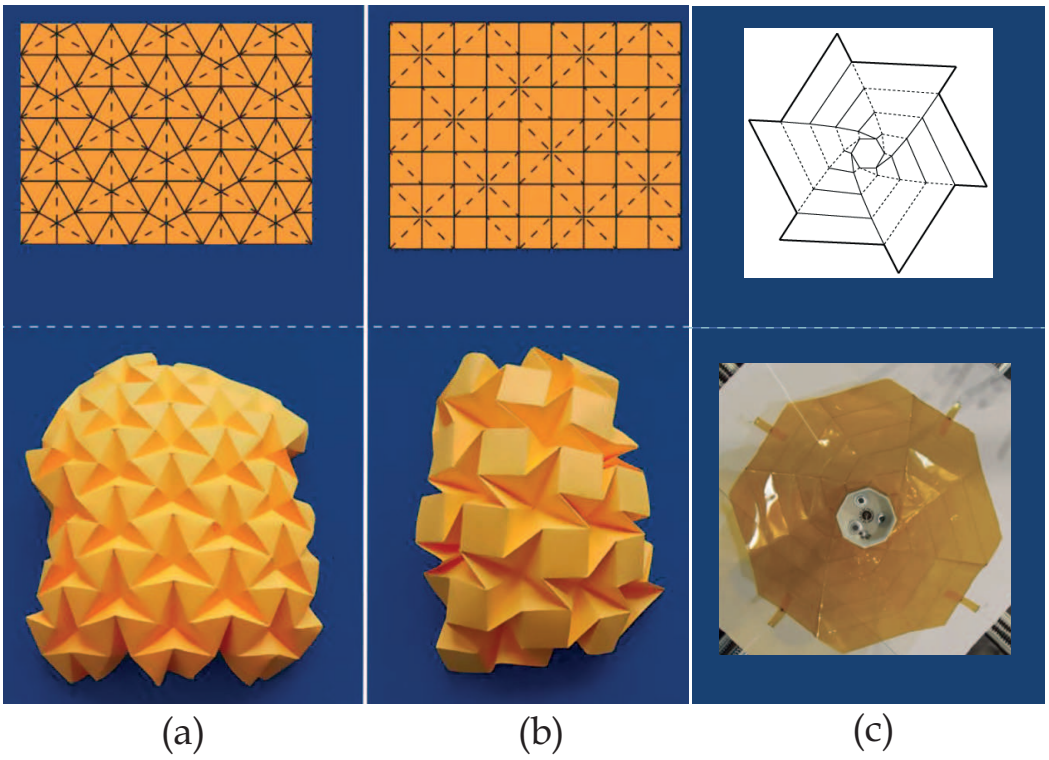

Figure 2.2: Crease patterns
(a) Resch [25] (b) Waterbomb [26] (c) Guest & Pellegrino [21]

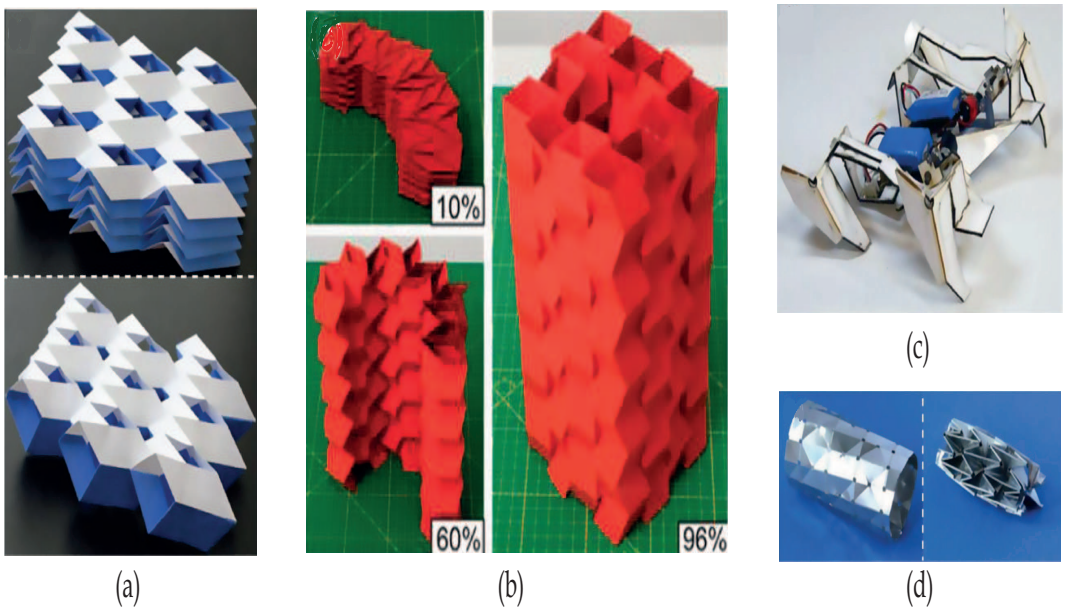

Figure 2.3: Applications of tessellated membranes
(a) paper versions of cellular metamaterials (b) a deployable paper structure based on origami zipper tubes [24] (c) a self folding robot [28] and (d) self-deployable origami stent graft based on the waterbomb pattern [26]

applications include self-folding robots and bio-medical devices as illustrated in Figure 2.3.

2.2 Studies on Fold-lines

The kinematics of folded membrane were explored mainly under the pseudo-rigidity assumption in the past [31], considering rigidity of faces on either side of creases and creases as the zone of concentrated strain and movement. This approach simplifies modelling but does not fully describe the degrees of freedom of these structures. It is now known that the movement depends not only on the creases but also on the flexibility of faces [32, 33]. This revelation has led to increased use of shell approach to modelling these membrane structures. However, to use the thin shell method for creased membranes, the initial imperfections should be quantitatively introduced to the numerical model [34].

2.2.1 Experimental studies

Efforts have been made to quantify the behaviour of creased membranes experimentally, especially to determine the material properties of the crease

region, which is highly non-linear and size dependent. Gough et al. [35] performed a series of experiments to measure global nonlinear properties of creased Kapton membranes. However, it was carried out at a relatively high stress range due to gauging difficulties. Hossain et al. [20] performed uniaxial tensile tests, also at a relatively high stress range on creased Kapton membranes and observed that creases offer permanent deformation and length shortening. Non linearity in material properties was confined to the crease region and elsewhere elastic behaviour was identified. Figure 2.4 shows the experimental setup and the stress - strain relationship recorded in the crease region (hyper-elastic) and membrane region (linear-elastic).

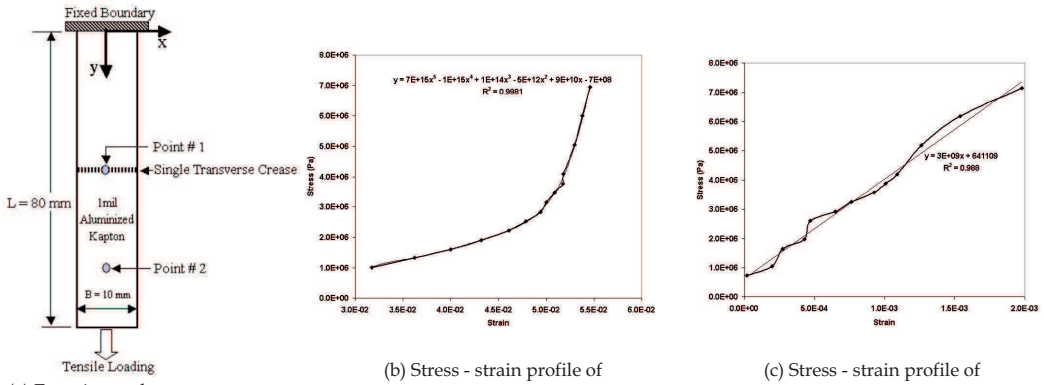

(a) Experimental setup

(b) Stress - strain profile of crease region (Point 1)

(c) Stress - strain profile of membrane region (Point 2)

Figure 2.4: Experimental investigations of tensile behaviour of Kapton [20]

Thiria and Adda Bedia [36] presented a model experiment to observe the relaxation mechanism of single creased membranes. In the experiment conducted with Mylar, two regimes of relaxation, the first due to stretching of the fold and the second narrow Arrhenius-like relaxation, were observed (see Figure 2.5).

Lechenault et al. [37] observed the behaviour of single creased membranes under external load and rotational stiffness offered by creases against deployment was quantified. Authors quantified the moment-rotation response of single folded 350 μm Mylar membranes using force sensors. A linear relationship of moment and angle was observed as shown in Figure 2.6. The authors also proposed a limiting value for dimensions of membrane specimens to be used in testing, below which bending of faces due to external loads can be ignored.

The studies highlight that due to the associated extreme compliance, experimental characterization of creased membranes is quite challenging. Hence

engineers also opt for analytical and numerical studies to understand the underlying mechanics of creased membranes.

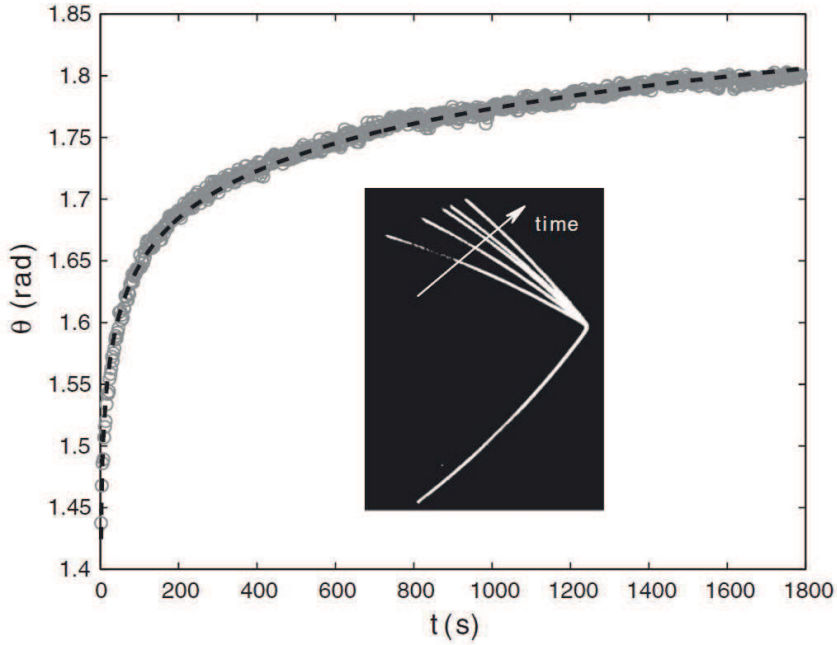

Figure 2.5: Time evolution of the angle of a crease made in a Mylar sheet of thickness 350 μm [36] (Inset: Superimposed images of the Mylar sheet during relaxation)

2.2.2 Analytical and numerical studies

MacNeal and Robbins [38] developed an analytical model for transversely creased tape under a tensile load based on elasto-plastic beam theory to predict the crease topology. From the topology, effective elastic modulus of creased tapes was predicted. Murphy et al. [39] extended this model for coated membranes. In these studies, the creased hinge was simply assumed to behave elastically initially and then become a perfectly plastic hinge beyond a certain load level. In the derivation, effect of creasing procedure and consequentially the residual stress during creasing were not considered. Woo et al.[40] developed a numerical model to determine the effective modulus of single creased thin membranes where the whole process of creasing and subsequent uniaxial tensile loading test were simulated considering elasto-plastic material properties for the membrane specimens.

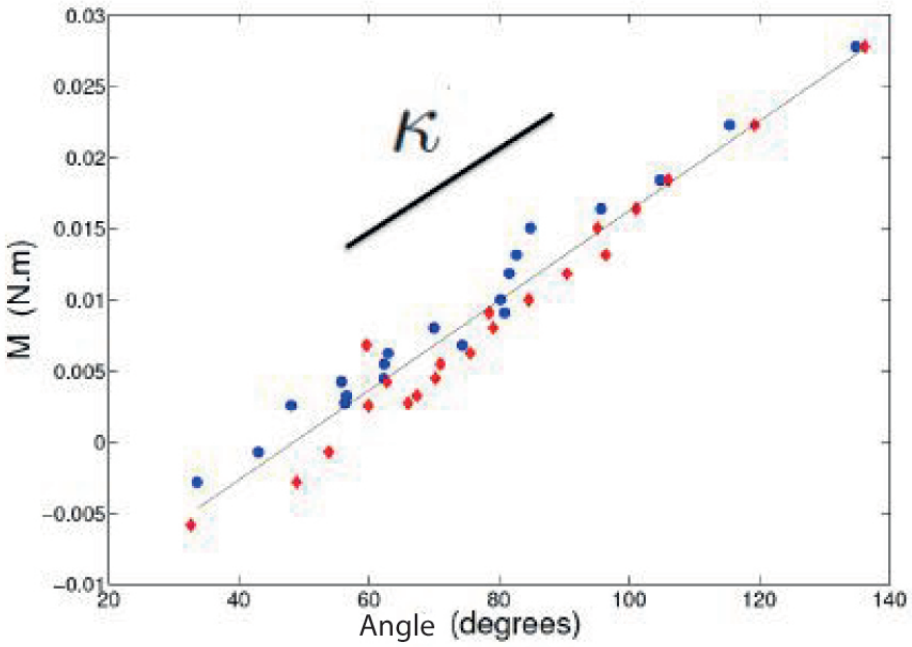

Figure 2.6: Moment - angle relationship for a Mylar sheet of thickness 350 μm [37]

These extensive studies highlight that understanding crease mechanics is essential to understanding the overall behaviour of membrane structures with crease network. The crease behaviour can be simplified to two key characteristics, relaxation mechanism as soon as the creasing load is removed and rotational resistance to opening by an external load.

2.3 Numerical Simulation of Creased Membrane Structures

It is evident that creases are influential in altering material state and mechanical response of creased membrane structures. Hence, deployment simulation of large creased membrane structures like solar sails, aimed at design optimization requires creases to be introduced into the thin-film for accurate prediction of deployment behaviour.

Characterizing the deployment behavior numerically requires determining the material properties of the film, the bending properties of the creases and contact response when the film comes into contact with itself. In employing shell approach to modelling these films, material properties and contact properties can be fed into the simulation with ground tests. However, capturing the fold-line behaviour in virtual simulations is challenging.

Sleight et al. [41] have developed separate virtual simulations for ground deployment test of a 10 m x 10 m sail by NASA. NEiNastran and Abaqus software packages were used for simulations. Liyanage and Mallikarachchi [42] in carrying out virtual simulations to assess the merit of spiral and circumferential folding patterns have considered ideal conditions of zero-thickness and no plastic deformation in the fold line. In both these studies, for simplification crease-mechanics were ignored.

One option is to represent creases with a moment−angle relationship like how it was done for simulations of the IKAROS solar sail mission [43]. However, the sail was modelled with membrane elements which failed to capture the bending of panels which is a key consideration as well. Papa and Pellegrino [44] used thin shells to model the membrane and introduced creases as kinks. This approach assumed the crease region to have the same stiffness as the base membrane. Further, it is tedious to employ this approach to model membranes with large number of creases.

Recently, Dharmadasa [16] has made an attempt to include fold line properties in virtual deployment simulation of a solar sail model. Creases were modelled with tie constraints and connector elements offered by Abaqus. The connectors can be defined with rotational stiffness. This enables the inclusion of rotational stiffness as well as the self-opening action due to creases in simulations.

Chapter 3

Predicting Mechanical Properties of Fold-Lines

This chapter focuses on predicting fold-line mechanics of single folded thin membranes using numerical simulations. The experimental study by Dharmadasa et al. [19] on thin Kapton membranes is chosen as a case study and the possibility of quantifying fold-line mechanics using an analytical model based on Elastica theory is explored.

3.1 Mechanics of Fold-Lines

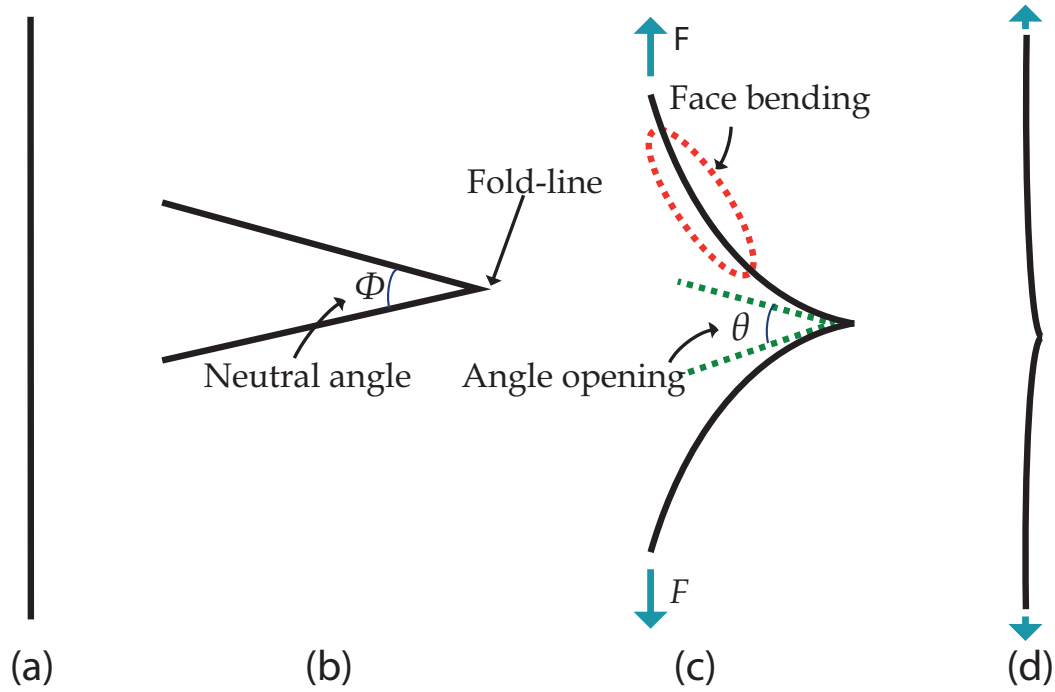

Figure 3.1: Geometric state of membrane
(a) initial stress-free state (b) new stress-free state after folding (c) unfolding due to external load (d) fully unfolded state

The focus of this study is the effect of fold-lines on the deployment

behaviour of creased membrane structures. The fold-line mechanics underlying while the creased membranes are unfolding were investigated in this regard. This underlying mechanics is twofold: 1) *Relaxation Mechanism* – the self-opening action exhibited by creased membranes as soon as the creasing load is removed (see Figure 3.1(a) and 3.1(b)) *Moment-Rotation Response* when opening with an external load (see Figure 3.1(c)).

The study of such mechanics at the microscopic scale is complex and is not under the scope of this study. A better understanding of the underlying mechanics from a macroscopic point of view can be achieved by studying membrane coupons with single straight fold. Further, it uncouples the effect of crease interaction and measurement difficulties present in a multiple-creased membrane.

3.1.1 Relaxation mechanism

Relaxation mechanism was observed by Papa and Pellegrino [44] in a membrane creased with a Miura-Ori folding pattern. Physical tests on single folded thin membranes have been conducted to quantify the relaxation mechanism by using opening angle at stress free state termed as Neutral angle (ϕ), as an index (see Figure 3.1(a)) [45, 19]. Mierunalan and Mallikarachchi [46] focused on predicting neutral angle through numerical simulations. Effects of folding pressure, material properties and thickness on neutral angle were explored, and a close agreement was achieved with the experimental results.

3.1.2 Moment-rotation response

The mechanical response of a creased membrane to an external load has two characteristics as illustrated in Figure 3.1(c). The first is the change in the angle of the fold, which is dependent on the material and fold preparation method. The second is the bending of the faces on either side of the fold-line, which is dependent on the flexural rigidity of the faces and boundary conditions. The internal resistant moment in the fold-line is a function of fold angle. An effort should be made to isolate this moment-rotation response of the fold-line from the bending of faces, as bending of faces is captured by employing shell approach to model membranes in numerical simulations.

Pradier et al. [47] and Dharmadasa et al. [19] utilized a simple experimental setup as illustrated in Figure 3.3 to characterise the moment-rotation response

using calibrated weights. In the experiments, selected membrane specimens were folded using a roller to form a straight fold-line in the middle. Then, one end of the folded membrane at stress free neutral angle state, was attached to a rigid frame using a low stiffness adhesive tape and the other end was loaded with prescribed calibrated weights progressively. The opening angle θ, was measured using digital images taken at each loading stage.

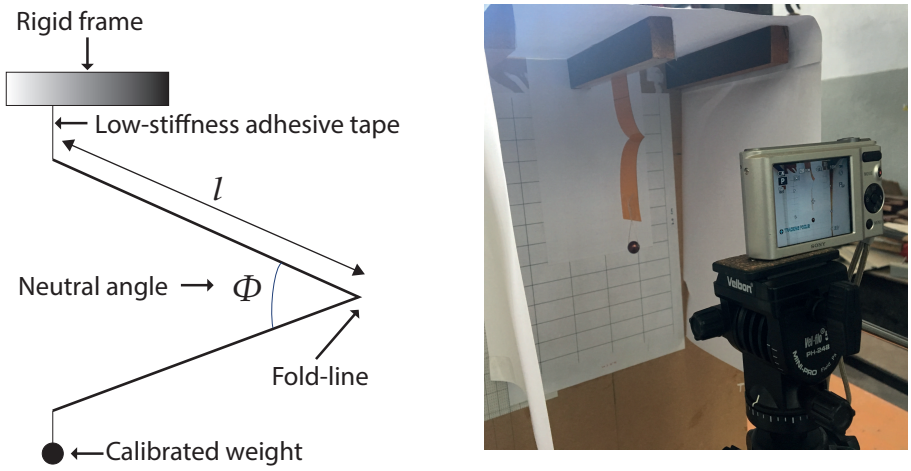

(a) Experimental setup

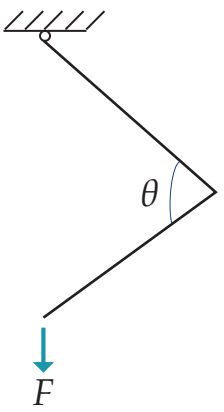

(b) Opening behaviour in [47]

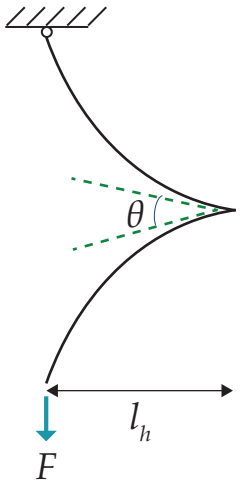

(c) Opening behaviour in [19]

Figure 3.2: Experimental investigations of moment - rotation response [47, 19]

The former study which was performed on printer paper, neglected the bending of faces by selecting specimens based on [37]. Hence, the moment at the fold-line due to applied load F was taken as $M = Flcos(\theta/2)$. However, in

the latter study which was performed on Kapton membranes, the deformed shape was as illustrated in Figure 3.1(c). Hence, in order to isolate the bending of faces, the moment was taken as in Equation 3.1,

$$M = Fl_h \tag{3.1}$$

Then a relationship between moment (M) and current opening angle of the fold (θ) was established as in Equation 3.2.

$$M = kw(\theta - \phi) \tag{3.2}$$

where ϕ is the neutral angle, w is the width of the membrane and k is the gradient of $M - \theta$ graph.

3.2 Elastica Theory

The movement of membrane can be regarded to be sufficiently slow compared to the characteristic times taken for elastic wave propagation, in the experiment carried out in [19]. Hence, membrane can be considered to be in static equilibrium at each loading stage. By taking advantage of this, it is possible to establish a relationship between F and θ. Since $l/t >> 100$ for the membrane specimens under consideration, Foppl - Von Karman plate theory can be used to analytically deduce the deformed topology of the membrane under tensile load.

However, by neglecting any out of plane curvature of the membranes and variance in thickness when loaded, the problem can be simplified to solving high deflection beam theory or Elastica theory. Taking advantage of symmetry about fold-line, one half of the membrane is treated as a 1-dimensional beam fixed to a rotational spring at a variable angle $\theta/2$ at each loading stage. The definition of curvature (κ) at any point along the deflected beam in Cartesian coordinates defined in Figure 3.3 is given in Equation 3.3.

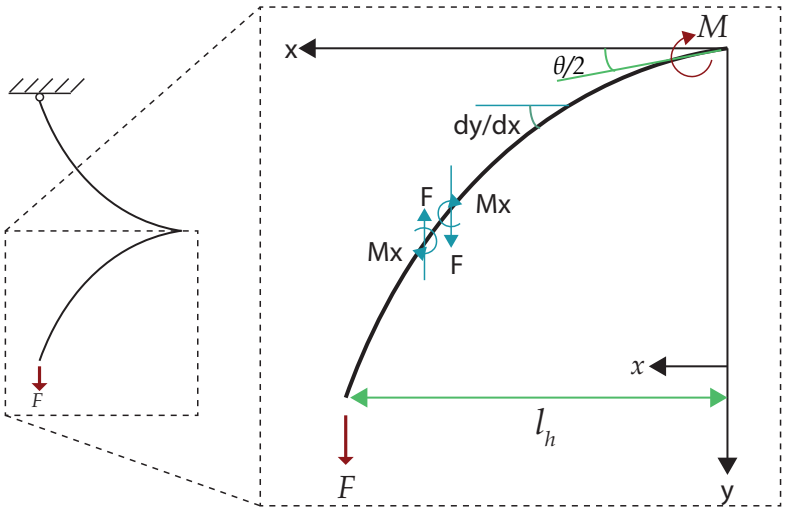

Figure 3.3: Idealized beam considering symmetry

$$\kappa = \frac{\frac{d^2y}{dx^2}}{\left(1 + \left(\frac{dy}{dx}\right)^2\right)^{\frac{3}{2}}} \tag{3.3}$$

The Euler-Bernoulli theory that relates bending moment (M_x) and curvature (κ) still holds for this highly deflected beam due to assumed small strain. This relationship for a beam with uniform elastic modulus (E) and second moment of area (I) is given in Equation 3.4.

$$M_x = \mathrm{E}I\frac{\frac{d^2y}{dx^2}}{\left(1 + \left(\frac{dy}{dx}\right)^2\right)^{\frac{3}{2}}} \tag{3.4}$$

By free body diagram, the bending moment at any point along the deflected beam is as in Equation 3.5.

$$M_x = F(l_h - x) \tag{3.5}$$

By combining Equations 3.4 & 3.5, we obtain Equation 3.6.

$$F(l_h - x) = \mathrm{E}I \frac{\frac{d^2y}{dx^2}}{\left(1 + \left(\frac{dy}{dx}\right)^2\right)^{\frac{3}{2}}} \tag{3.6}$$

Equation 3.6 is a second order non-linear differential equation and the exact solution is not present. However, treating it as a boundary value problem, a solution can be obtained. MacNeal and Robbins [22] have obtained a solution by imposing boundary conditions of $\theta/2$ on one end and the invariance in length as in Equation 3.7.

$$\frac{dy}{dx} = \sin^{-1}\left(\frac{F}{2\mathrm{E}I}\left(x - l_h\right)^2\right) \tag{3.7a}$$

$$\text{where} \quad l_h = \sqrt{\frac{2\mathrm{E}I}{F}\left(1 - \sin(\theta/2)\right)} \tag{3.7b}$$

Though this solution requires θ to be input which can be only obtained through simulations or experiments, by substituting θ, this will serve as a check for l_h, used in determining moment in the fold-line as per Equation 3.1.

3.3 Finite Element Simulation

To predict the moment-rotation response numerically, finite element models of Kapton thin membranes were set-up in commercial finite element package Abaqus/Standard [18]. Though 40 mm long and 20 mm wide membrane coupons were used in [19], taking advantage of symmetry about fold-line, only one half of the membrane coupons were modelled. Since the membrane coupons of concern are predominantly under bending stress state during the entire simulation, plane strain condition was assumed. Hence only the cross section of the membrane was modelled with 2-dimensional plane strain elements.

Accordingly, the type of element selected for the simulation was four-node plane strain elements with incompatible mode (CPE4I). The incompatible mode enables the use of lesser number of elements compared to elements with first order reduced integration and is cost-effective compared to second order

elements which are commonly used to overcome shear locking problem associated with in-plane bending. Minimization of distortion was achieved by having a finer mesh closer to the creased region and a coarser mesh towards the free end of the membrane, resulting in better accuracy(see Figure 3.4). A typical finite element model consisted of 9898 nodes and 8631 plane strain elements with a minimum length of 0.8 μm.

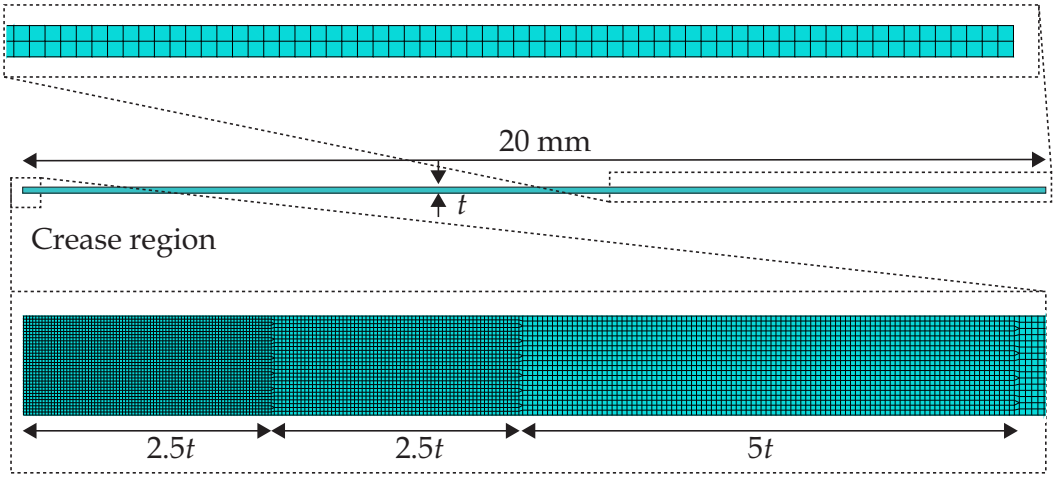

Figure 3.4: Mesh arrangement from the finite element simulation to determine moment - angle response of a single crease

The folded configuration of the membrane needs to be computed first, in order to generate its moment rotation response. Though a rolling procedure was adopted in the experimental study [19], the implementation of such procedure in numerical simulations is complex. Hence, the folded configuration or creased geometry was achieved through the methodology set out in [46]. Three different creasing gauges, $d = 1.5t, 2t \; and \; 2.5t$ were chosen to generate different creased geometries ($\phi/2$) in the range of neutral angles observed in experimental study, where t is the membrane thickness. Once the creased geometry was achieved, the membrane was subjected to sequential tensile loading (F) at the free end to simulate the experimental procedure in [19]. A loading regime ranging from 0.00001 N to 10 N was chosen to maintain predominant bending stress state. At each loading stage, θ and l_h were recorded numerically. Figure 3.5 illustrates the employed simulation sequence.

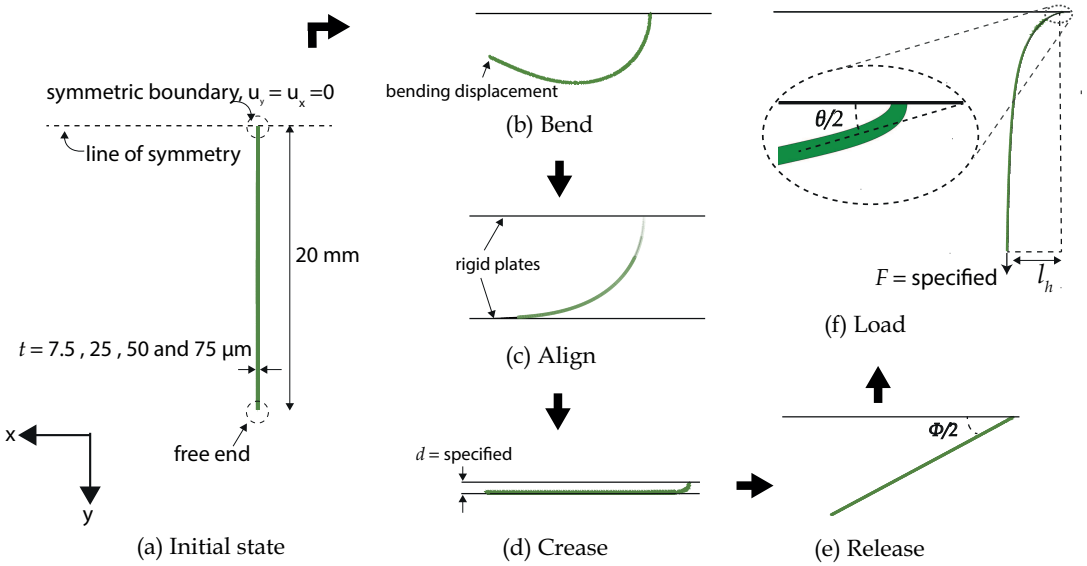

Figure 3.5: Snapshots from the finite element simulation to determine moment - angle response of a single crease

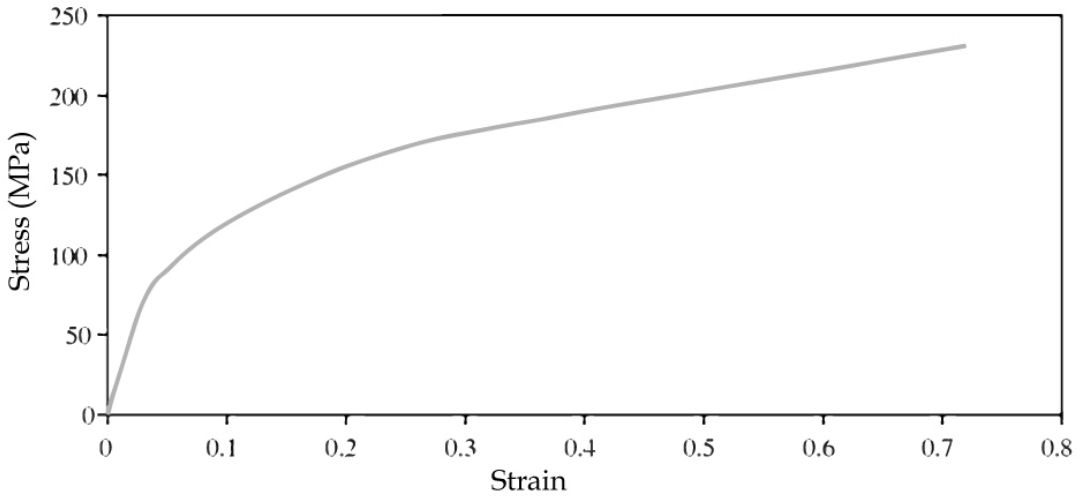

Figure 3.6: Stress - strain curve for Kapton - type HN film [17]

In this study, 7.5 μm, 25 μm, 50 μm and 75 μm thick Kapton - type HN membranes were simulated. Figure 3.6 shows the stress strain curve of Kapton membrane [17]. The specification of true stress, true strain and true plastic strain in material definition is required by Abaqus. Accordingly, for the conversion of nominal stresses (σ_{nom}) and normal strains (ε_{nom}) from Figure 3.6 to true stresses (σ_{tru}), true strains (ε_{tru}) and plastic strains (ε_{pla}), Equations 7, 8 and 9 were utilized. Table 1 summarizes the Kapton material properties used in the simulation.

Table 3.1: Material properties of Kapton used in the finite element simulation to determine moment - angle response of a single crease

Density (kg/m^3)	1420
Elastic modulus (MPa)	2500
Poisson's ratio	0.34
Yield stress (MPa)	69
Yield strain	0.03
Ultimate stress (MPa)	231
Ultimate strain	0.72

Abaqus/Standard solver with Newton-Raphson time integration was used for simulations owing to the two-dimensional nature of the problem with no significantly large deformations. However, the resulting complications of instability and localized deformation (on contact and application of displacement at a single node respectively) with Static/General analysis step had to be overcome by using **STATIC, STABILIZE* option. A stabilization factor ranging from 2 x 10^{-7} to 2 x 10^{-5} and a reasonable time scale from 1.0s to 5.0s for varying creasing gauges were used based on a trial and error process.

3.4 Results and Discussion

Figure 3.7 shows the creased geometry and the tensile geometry of 25 μm Kapton membrane subjected to three different creasing gauges (1.5t, 2t and 2.5t) and a subsequent tensile load, F of 0.4 N. The crease, takes the form of a kink (locally) as seen in Figure 3.7. However, the experimental work in [19] did not capture such fine details. Hence, to maintain consistency, $\phi/2$ and $\theta/2$ were measured by drawing a tangent to the straight region immediate to the kink region as shown in Figure 3.7.

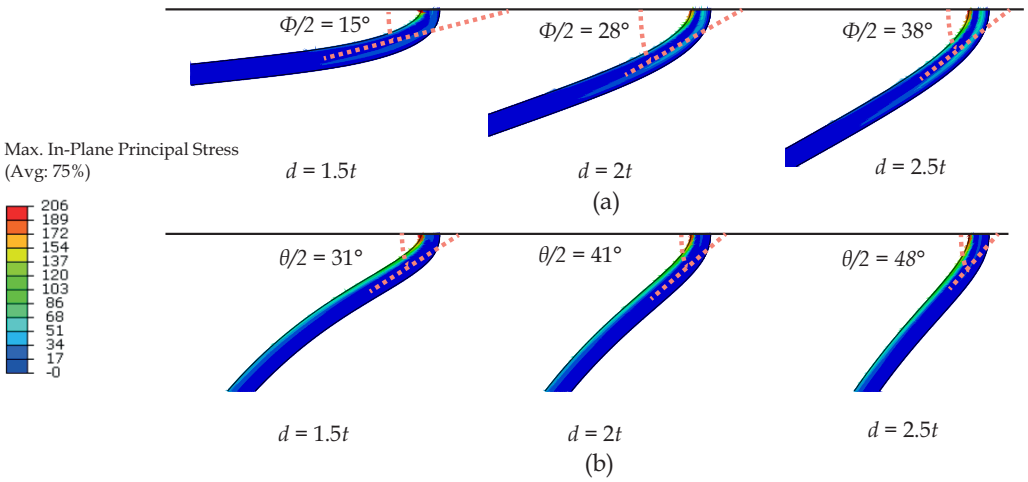

Figure 3.7: Deformed shape of 25 μm Kapton membrane
(a) when creased to different creasing gauges (b) when subsequently subjected to 0.4 N tensile load

Figures 3.8, 3.9, 3.10 & 3.11 show the moment - rotation response of Kapton membranes of four thicknesses subjected to three different creasing gauges. Moment at each loading stage was calculated using Equation 3.1 and divided by the width of the membrane coupon (20 mm) to obtain the moment per unit width. Distance from fold-line to loaded end, l_h in Equation 3.1 was numerically recorded at each loading simulation along with the opening angle, $\theta/2$ as indicated in Figure 3.5.

Moment - rotation responses of all thicknesses generally have three phases. In the initial phase, there is no angle opening with increasing moment. This increase in moment is due to local bending at the edge of the membrane. This is pronounced in 7.5 μm Kapton membrane. There is a drop in transition from first phase to second phase. This is due to the membrane undergoing high deflection and transforming to a vertical asymptote towards the loaded end, causing a sudden decrease in l_h, thus M. In the second phase, all three thicknesses exhibit an approximately linear moment rotation response with almost similar gradient for all three creasing gauges. In the third phase, moment - rotation response undergoes a decrease. Careful observation of the simulation revealed that with increasing load, the membrane undergoes axial extension making the dominant bending assumption void. Hence, the results in the third phase are unreliable.

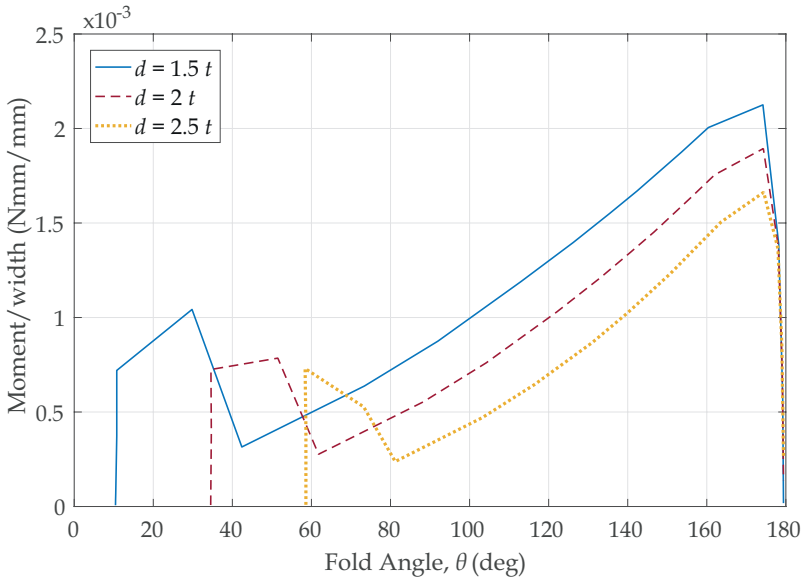

Figure 3.8: Moment - angle relationship for Kapton 7.5 μm

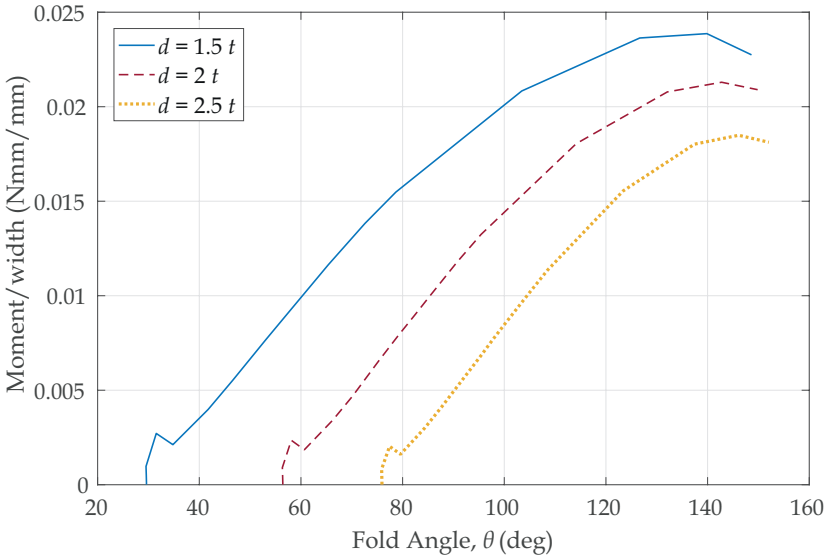

Figure 3.9: Moment - angle relationship for Kapton 25 μm

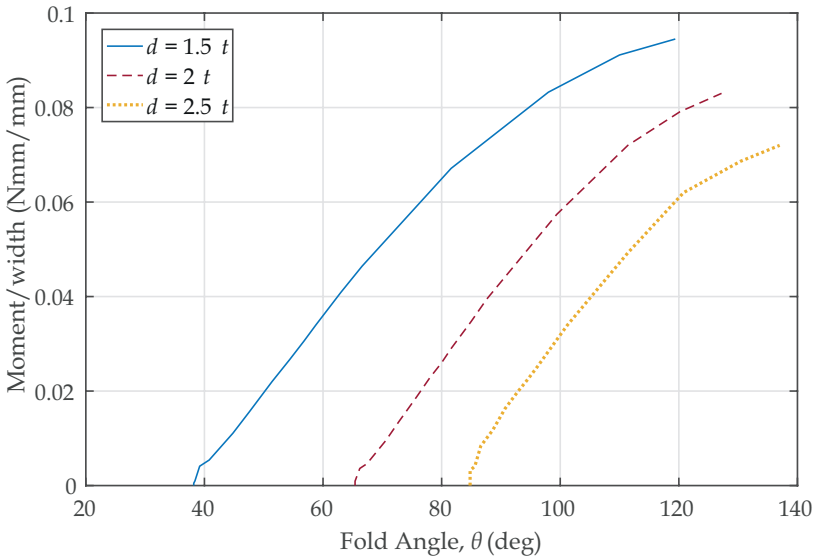

Figure 3.10: Moment - angle relationship for Kapton 50 μm

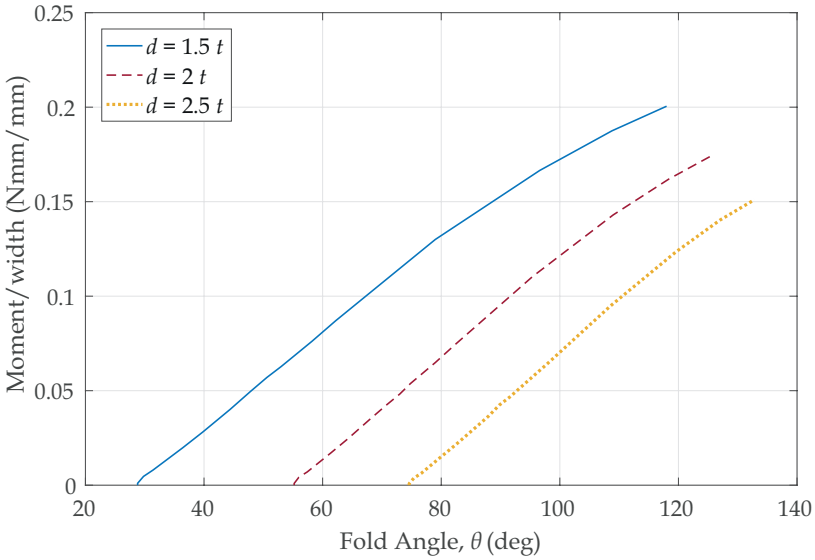

Figure 3.11: Moment - angle relationship for Kapton 75 μm

Only the linear phase was observed in [19] due to the limited availability of calibrated weights. Table 3.2 presents a comparison of fold-line stiffness (k) calculated from the gradient of the linear region of the moment-rotation plots (Figure 7) to that from the experiments. For a particular thickness, the average fold-line stiffness from the 3 creased gauges is presented.

Table 3.2: Comparison of fold-line stiffness

Membrane thickness	**Fold-line stiffness**(N/deg)	
	Experiment [19]	Simulation
7.5 μm	-	0.000017
25 μm	0.00015	0.00003
50 μm	0.0006	0.0010
75 μm	0.0025	0.0026

The values obtained from the simulations were observed to be of the same order as the experimental values [19] for membrane thicknesses 25 μm, 50 μm and 75 μm, with no significant effect imposed from the varying neutral angles (ϕ) which was observed in experiments as well.

Figure 3.12 shows a comparison between l_h obtained from simulating 25 μm Kapton membrane creased to creasing gauge of $2t$ and the solution from Elastica for the same (Equation 3.7b), against tensile load, F. For a loading regime less than 0.02 N, there is a significant deviation between the two methods. This is due to the assumption in Elastica that towards the loaded end, membrane will form a vertical asymptote. However, in the simulation there were no significant deflections observed for loads below 0.02 N. For loads above 0.02 N, a fair agreement can be seen. A slight deviation is still existent as Elastica assumes the fold-line to be a hinge whereas in the simulation the fold-line takes the form of a kink as in Figure 3.7.

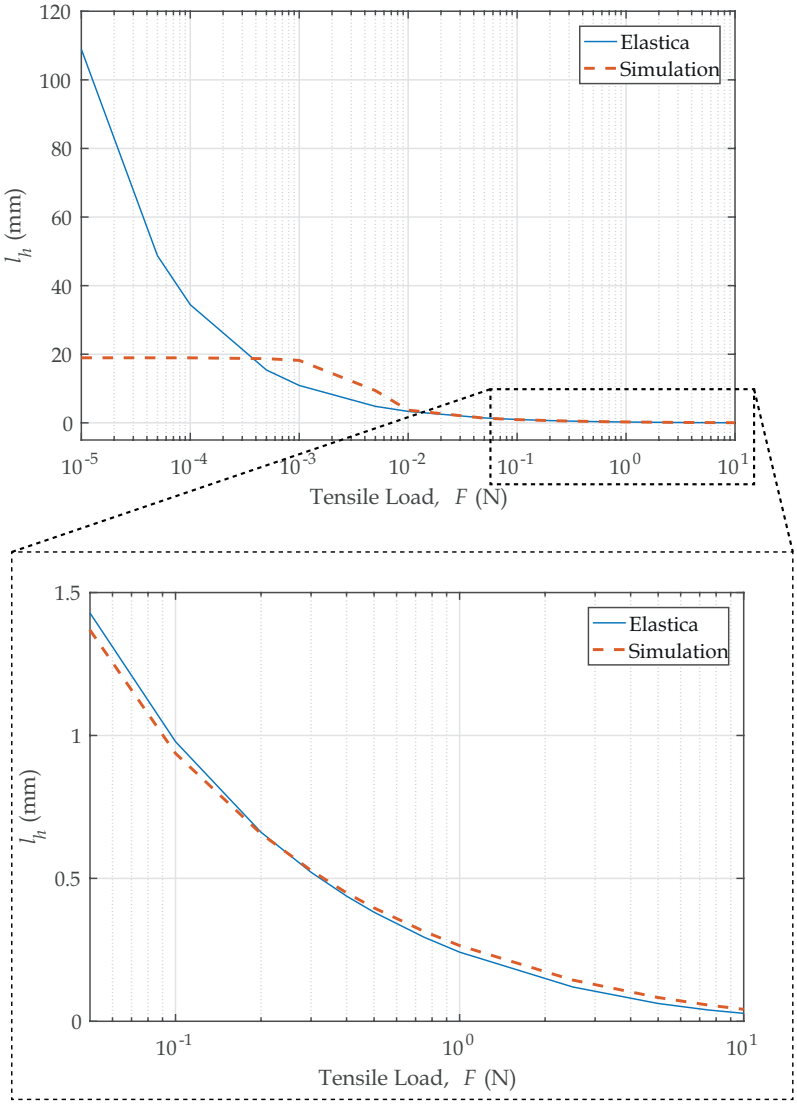

Figure 3.12: Comparison of l_h values from simulation and Elastica theory

Chapter 4

Implementation in Finite Element Package

In this chapter, how the fold-line mechanics predicted in Chapter 3 are to be incorporated in numerical simulations of folded membranes is discussed. For demonstration, unfolding of a single folded Kapton membrane to an external tensile load is simulated and validated against the experiments carried out by Hossain et al. [20].

4.1 Connector Element

Taking advantage of negligible thickness compared to other two dimensions of the films, it is convenient to model them with shell elements. Modelling the membrane panels with shell elements makes it possible to capture the panel bending as illustrated in Figure 3.1. The width of the crease line itself is in the order of thickness of these films [45]. Hence, in view of its small width, crease line could be conveniently represented by connector elements, connecting two adjacent shell elements (see Figure 4.1). In this study, it is proposed to represent the crease line with a series of 2-noded connector elements with zero thickness, connecting two adjacent Kirchhoff shell elements (see Figures 4.1 & 4.2).

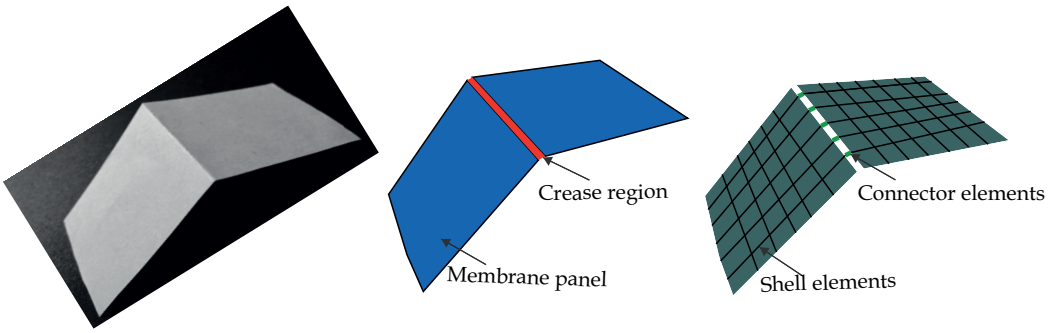

Figure 4.1: Representation of folded membrane with shell and connector elements

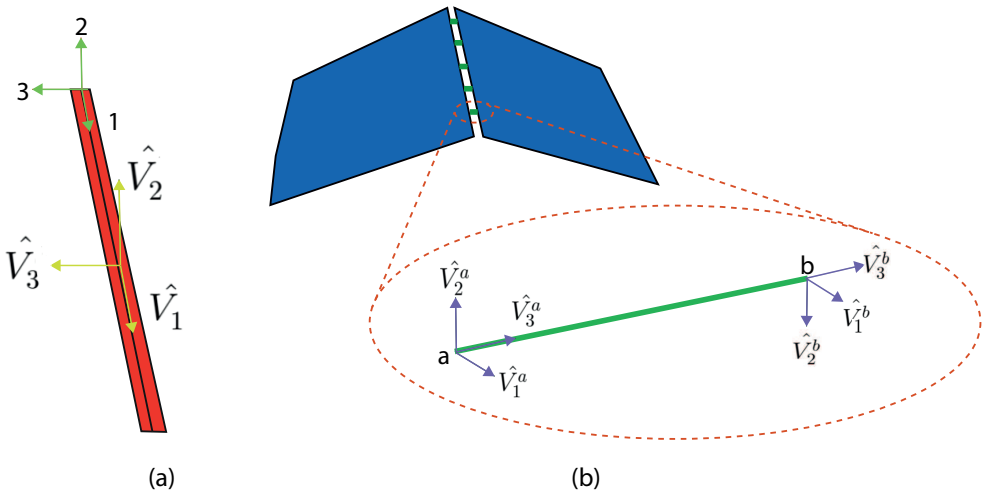

Figure 4.2: Local axes and vector definitions for (a) crease region (b) a connector element

The crease region connecting two membrane panels is illustrated in Figure 4.2(a) with local axes and corresponding vector definitions. Since creasing weakens the bending properties along crease lines, only rotations about 1 can be expected to be large. In fact, this relative rotation has been considered to be the dominant factor affecting rotational resistance to opening by an external load in Chapter 3. As discussed, mechanics of fold-line under consideration are associated with opening angle of the fold and resisting moment due to internal stresses in the crease. Hence both responses discussed in Section 3.1 could be represented by the constitutive equation for moment-angle about 1 as in Equation 4.1.

$$M = \begin{cases} k_r\theta, & \text{if} \quad \theta < \phi \\ k_o(\theta - \phi), & \text{if} \quad \theta \geq \phi \end{cases} \tag{4.1}$$

where θ is the opening angle of the fold, ϕ is the neutral angle, k is the fold-line stiffness and subscripts r and o indicate relaxation and opening respectively.

This constitutive model in Equation 4.1 could be implemented in connector elements by constraining rotations about 2 and 3 axes and imposing free rotation about the shared axis 1. The two kinematic constraints to be imposed are given by Equation 4.2.

$$\hat{V_1^a} \cdot \hat{V_2^b} = 0 \quad and \quad \hat{V_1^a} \cdot \hat{V_3^b} = 0 \tag{4.2}$$

Node b can rotate about the shared local axis 1. The rotation θ of the local directions of node b relative to node a is given by Equation 4.3.

$$\theta = -\tan^{-1}\left(\frac{\hat{V_2^a} \cdot \hat{V_3^b}}{\hat{V_3^a} \cdot \hat{V_3^b}}\right) \tag{4.3}$$

where θ is measured in anticlockwise sense of angle of rotation of $\hat{V_2^a}$ and $\hat{V_2^b}$ about $\hat{V_1^a}$. Hence the connector constitutive rotation can be described by Equation 4.4

$$\beta = \theta - \beta_i \tag{4.4}$$

where β_i is the initial angular position and at closely creased state $\beta_i = 0$. this leads to $\beta = \theta$. Kinematic moment in the connector is given by Equation 4.5.

$$M_c = M_1 \hat{V_1^a} \tag{4.5}$$

By combining Equations 4.1 & 4.5, the constitutive model reduces to Equation 4.6.

$$M_c = \begin{cases} k_r \theta \hat{V_1^a}, & \text{if} \quad \theta < \phi \\ k_o(\theta - \phi)\hat{V_1^a}, & \text{if} \quad \theta \geq \phi \end{cases} \tag{4.6}$$

Hence, if both k_r and k_o are known and assigned to connector elements, the mechanics of fold-lines can be captured by the proposed method.

4.2 Implementation in Abaqus

In this section, an attempt is made to simulate the unfolding of single-folded thin membranes using the above proposed connector element in a commercially available finite element analysis software. Abaqus/FEA package was selected in this regard because of the robust algorithm involving connectors and contact simulation. Furthermore, it is widely used by the aerospace community. For the proposed technique to be a robust solution, it should be able to capture both behaviour within the fold-lines as well as behaviour of the membrane on either side of a fold-line, while unfolding. Hence in this section, performance of single folded membranes with the proposed technique, unfolded when subjected to tensile loads has been simulated. The results are validated against the experiments performed by Hossain et al. [20]. A comparison between the simulation techniques presented in [20, 15] and the proposed technique is also presented.

4.2.1 Finite element model of single folded membrane

A rectangular Kapton coupon folded in the middle with dimensions of 10 mm X 80 mm and thickness of 25 μm was modelled. Linear three-node shell elements (S3) were used for the shell portions in all the simulations. For bending simulations with contact, S3 elements have proven to be cost effective when compared to fully integrated quadrilateral elements (S4) and accurate by eliminating hour-glassing when compared to quadrilateral elements with reduced integration (S4R). However, for better accuracy distortion should be minimized. This was achieved by having a finer mesh closer to fold-line where high bending is expected and a coarser mesh towards the ends of the membrane. A typical finite element model consisted of 1618 nodes and 2964 shell elements with a minimum length of 0.25 mm.

The properties of Kapton used in the simulation are given in Table 4.1.

Table 4.1: Material properties of Kapton used in the finite element simulation of unfolding of single folded membrane

Thickness (μm)	25
Density (kg/m^3)	1420
Elastic modulus (MPa)	2500
Poisson's ratio	0.34

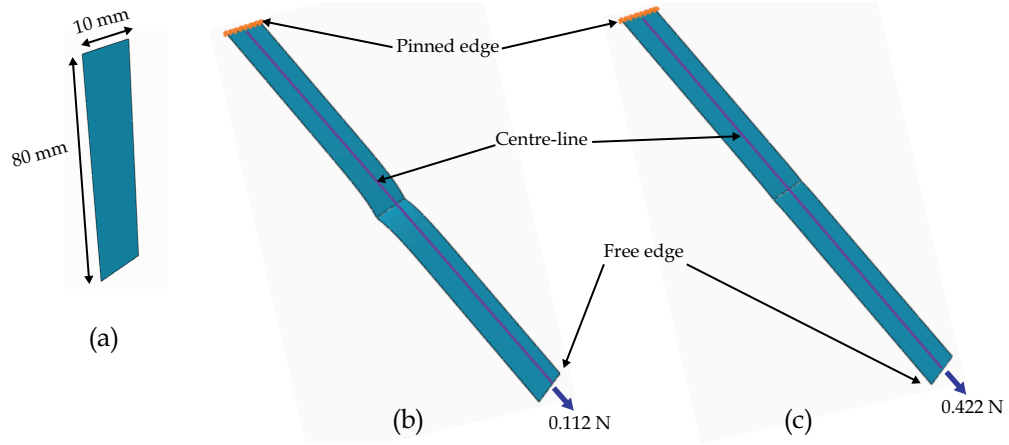

Figure 4.3: Simulation sequence for unfolding of single folded membrane (a) initial folded state (b) unfolding to 0.112 N tensile force (c) unfolding to 0.422 N tensile force

The simulation sequence was selected to follow the tensile testing experiment procedure discussed in [20] and illustrated in Figure 4.3. In the initial configuration the single-folded Kapton membrane is fully folded, i.e the fold angle $\theta = 0$. One end of the membrane was restrained with a pinned boundary condition allowing it to freely rotate while the other end was unrestrained. From the initial configuration, two tensile point loads of 0.112 N and 0.422 N were applied sequentially at the center of the free edge. Axial displacement in the loading direction of selected points lying on the centre-line of the membrane (see Figure 4.3) was recorded considering initial folded state as the base at both loading stages.

Since this is a simple simulation with no significantly large deformations, Abaqus/Standard solver with Newton-Raphson time integration was used. However, high curvature bending close to fold-line and application of load at a single node presented problems with instabilities and localized deformation respectively with Static/General analysis step. To stabilize the computation, the **STATIC,STABILIZE* option was used while maintaining the damping coefficient, just small enough for the computations to continue. Non-linear geometry option was used to capture the large deflections of the shell portions.

Modelling the fold-line

Three different approaches were followed to model the fold-line in the simulation as shown in Figure 4.4.

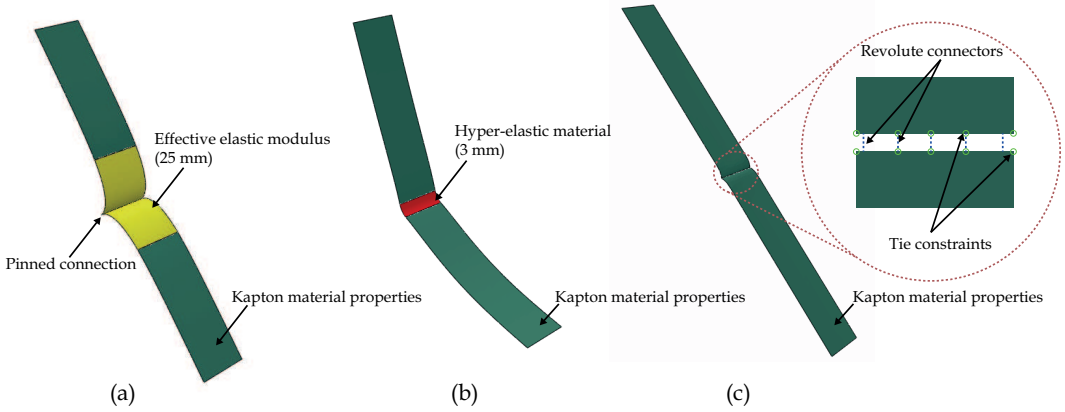

Figure 4.4: Different techniques used to model fold-line

(a) With effective modulus for crease region

In this approach, the methodology set out in [15] was followed. The folded membrane was modelled with two shell portions. The connection between two shell portions was established by using *TIE constraints without rotational degrees of freedom, simulating pinned joint. Crease region, extending over a distance of $500t$ on either side of fold-line was modelled with general purpose S3 elements similar to the shell portions but assigned with effective material properties obtained from experiments carried out by Cai et al. [15]. This modelling technique is illustrated in Figure 4.4(a).

(b) With hyper-elastic material properties for crease region

In this approach, the methodology set out in [20] was followed. The creased membrane was modelled as a single part with S3 elements with crease region, extending over a distance of 1.5 mm on either side of fold-line, and was assigned with hyper-elastic material properties. For evaluating the hyper-elastic material model to be used, Evaluate option in Abaqus was used. Fifth order reduced poynomial hyper-elastic material model that best fitted with the material test data obtained from experiments carried out by Hossian et al. [20] was used. Figure 4.5 shows the result from the evaluation procedure. This modelling technique is illustrated in Figure 4.4(b).

(c) Proposed technique

In this approach, the folded membrane was modelled with two shell portions. The connection between two shell portions was established by using **TIE constraints* without rotational degrees of freedom. Connectors were used to

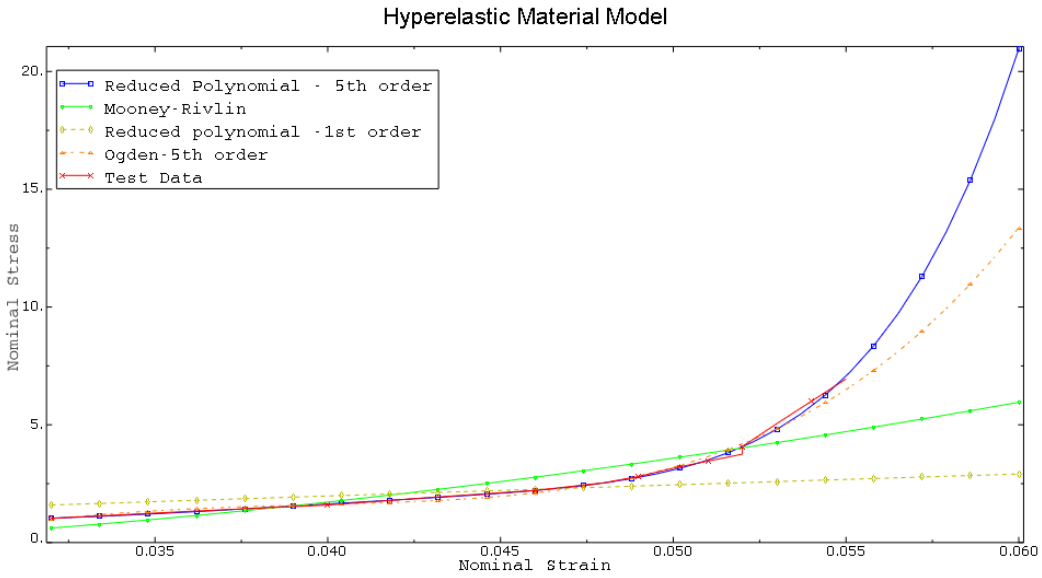

Figure 4.5: Results from hyper-elastic material model evaluation

incorporate the rotational stiffness of folds. *Revolute* type two-node 3D connector elements (CONN3D2) were used to model the connectors. As discussed in Section 4.1, only the rotation about the fold-line dominates the mechanics of fold-lines. *Revolute* type connector elements allow the user to allow a single desired rotational degree of freedom between two points and define rotational elasticity to account for rotational response of creases, that can be used for this purpose. **CONNECTOR, ELASTICITY* behaviour was assigned to connector elements to account for k_r and k_o, given in equation 4.6. In this case, it was considered as $k_o = k_r = k$ assuming a similar behaviour of Kapton to that of Mylar observed in [37] (see Figure 2.6). This assumption was made as there are no experimental data on k_o. The fold-line stiffness (k) was accounted for by using linear rotational elasticity. The value of k was obtained from Table 3.2. The total rotational stiffness of the fold-line was uniformly distributed among all the connectors along the fold-line. A sensitivity analysis on the number of connectors showed that with increasing number of connectors, the stress distribution tend to be uniform along the fold-line, compared to when fewer number of connectors are used which result in the concentration of stresses at the connected nodes. Based on the sensitivity study, 5 connectors were used. This modelling technique is illustrated in Figure 4.4(c).

4.2.2 Results and Discussion

Figure 4.6 shows a comparison of the axial displacement in the loading direction for the load case of 0.422 N with respect to the load case of 0.112 N, measured along the centre-line experimentally [20] with the simulated responses. This axial displacement was calculated as the difference in axial displacement in the loading direction from the initial folded state, between load cases of 0.422 N and 0.112 N. In addition, two extreme cases where fold-line is idealized as pinned joint (minimum rotational stiffness) and welded joint (maximum rotational stiffness) are also presented. The results are plotted against non-dimensional length (L^*) which indicates the location from the pinned end as a ratio of the overall length of the coupon (80 mm), of the selected points (to measure axial displacement) in the initial pristine state before creasing. The location of the fold-line is at a non-dimensional length of $L^* = 0.5$ (corresponding to 40 mm).

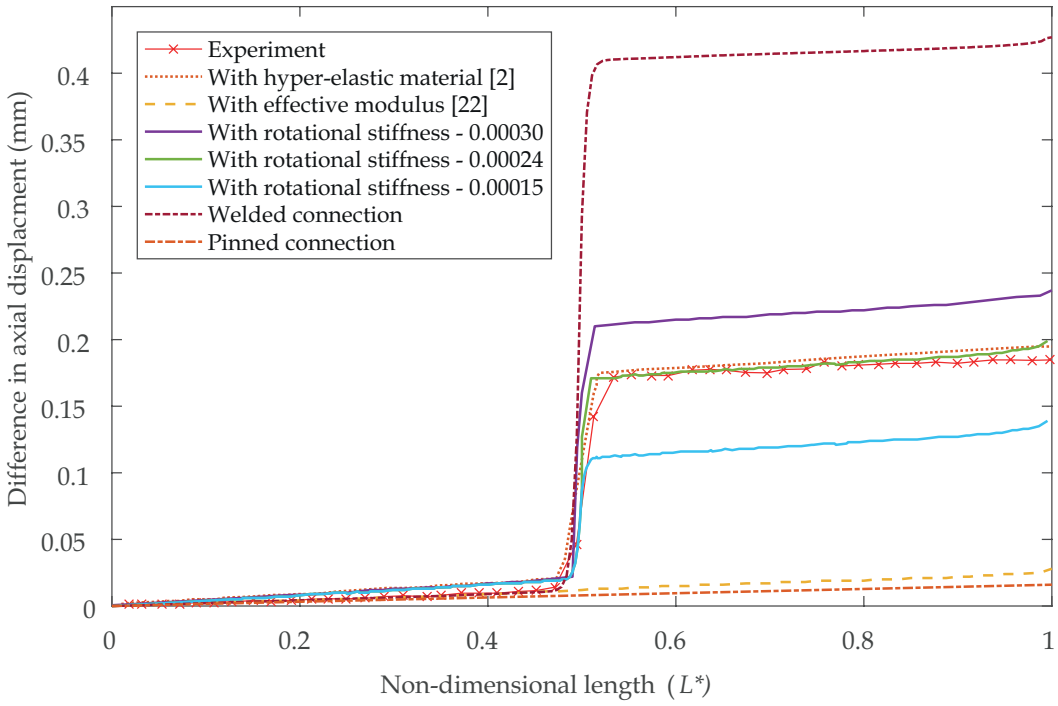

Figure 4.6: Comparison of difference in axial displacement between 0.422 N loading stage and 0.112 N loading stage

A "jump" in the experimental observation close to $L^* \approx 0.5$ corresponds to crease opening at 0.422 N loading stage from 0.112 N loading stage. The figure shows that the extreme cases of pinned and welded connection act as lower and upper bounds for the axial displacement respectively, with significant deviation

from actual behaviour. Welded connection gives a significantly higher estimation of crease opening (jump), whilst pinned connection fails to capture the crease opening. The technique proposed by Cai et al. [15] yields axial displacement close to that of pinned connection as this technique is also unable to capture the crease opening. Hence this technique cannot be used for our purpose.

Use of connector elements with rotational stiffness is able to capture the crease opening. However, use of rotational stiffness determined experimentally by Dharmadasa et al. [19] (0.00015 N/deg) and through simulations in the present work (0.0003 N/deg) give a slightly lower and higher estimation of crease opening respectively. This may be due to the assumption made that the neutral angle of the folded membrane is 0. This assumption was made since the neutral angle was not recorded during the experiment. Dharmadasa [16] observed that though the rotational stiffness is independent of the neutral angle, the resistant moment exerted by crease-line depends on the neutral angle as in Equation 4.1. Inputting the correct neutral angle might give a reduced crease opening as the resistant moment decreases. Following a trial and error procedure of using rotational stiffness in between the above values, an effective rotational stiffness of 0.00024 N/deg (that accounts for the neutral angle effect) gives a much closer estimation of crease opening.

The technique proposed by Hossain et al. [20] estimates the crease opening by axial extension of the hyper-elastic region and yields close agreement with experimental observations. However, for different loads, the hyper-elastic region length of 3 mm used in the simulation requires further calibration to match the results. Also at much smaller loads, it fails to capture the actual deformed geometry of the folded membrane. Figure 4.7 shows that the use of this technique gives an almost fully unfolded shape whereas it is not the actual deformed shape. Hence, this technique is suitable to study the behaviour of creased membranes in the fully deployed state but cannot be used for our purpose of predicting deployment behaviour of multiply creased membranes.

Another merit of the proposed technique is that it is cost effective to employ in modelling membranes with large no of creases. It should also be noted that the use of shell elements to model the membrane panels in all the simulations has captured the axial displacement due to bending or axial extension of the

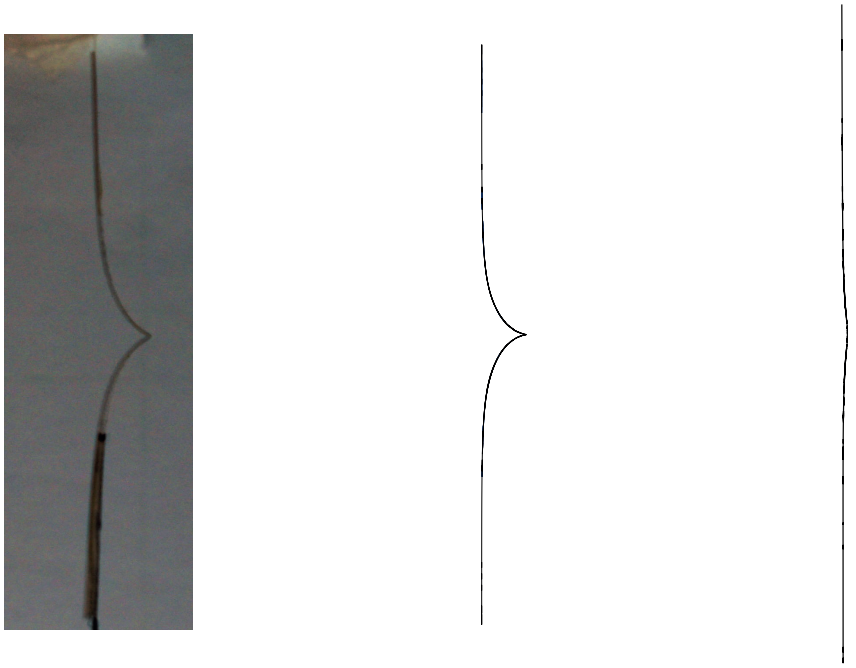

(a) Experiment (b) Proposed technique (c) Hossain et al. [2]

Figure 4.7: Comparison of deformation profiles for an external load of 0.002 N

membrane panel when subjected to external loads as well, thus giving closer results to experimental observations.

Chapter 5

Quasi-static Deployment Simulation of a Solar Sail

In this chapter, an attempt is made to develop a numerical model of complete solar sail with the proposed simulation technique to incorporate fold-line mechanics presented in Chapter 4 to study the deployment behaviour. The simulated response is compared against physical experiments carried out by Arya and Pellegrino [48].

5.1 Crease Pattern

For this purpose, a model of thin membranes wrapped around a polygonal hub based on the crease pattern proposed by Guest and Pellegrino [21] were utilized. This crease pattern algorithm takes four inputs: the number of sides of the polygonal hub (N), radius of circumcircle of the polygonal hub (R), the spacing between adjacent layers in the folded configuration (u) and the number of radial tabs (j). A solar sail model was created setting the parameters as given in Table 5.1. The fully deployed diameter (D_f) was around 265 mm.

Table 5.1: Parameters used to generate Solar Sail Model

t (μm)	25
N	8
R (mm)	20
u (μm)	50
j	8

In cylindrical coordinates defined at the centre of the hub as indicated in Figure 5.1(d), the coordinates of vertices P_{ij}, where i corresponds to fold-line and j corresponds to the vertex in the fold line, are given by Equation 5.1.

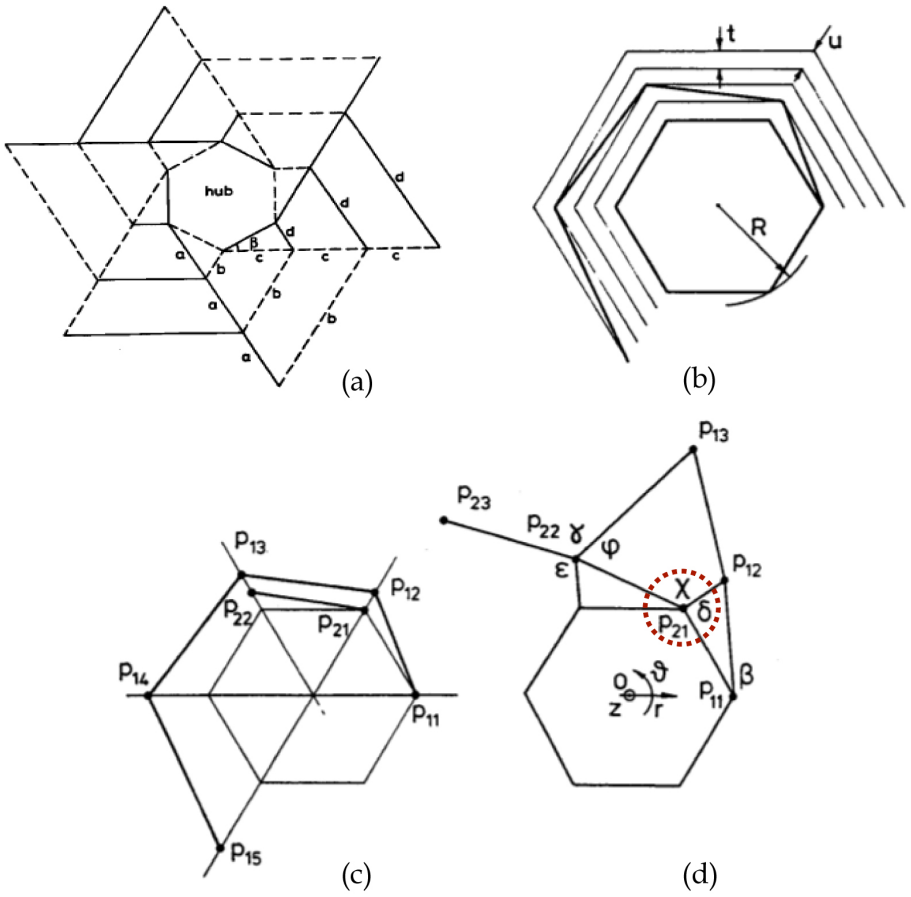

Figure 5.1: Crease pattern [21]
(a) crease pattern for n = 6 (b)plan view of fold lines in wrapped configuration (c) location of vertices P_{ij} in folded configuration (d) location of vertices P_{ij} in deployed configuration

$$P_{ij} = \begin{pmatrix} R + (j-1)s \\ 2(j-1)\pi/N \\ z_j \end{pmatrix} \tag{5.1}$$

The only unknown coordinate in the above is the z coordinate as other two coordinates can be simply obtained by substituting values from Table 5.1. In order to find the z coordinates (z_j), the angular relationship at a vertex in the deployed state can be used (see Figure 5.1(d)). This yields the following four simultaneous equations with four unknown terms, β, δ, χ and z_j.

$$\beta = arccos\left(\frac{(P_{12}-P_{11}).(P_{21}-P_{11})}{||P_{12}-P_{11}||\,||P_{21}-P_{11}||}\right) \tag{5.2a}$$

$$\chi = arccos\left(\frac{(P_{22}-P_{21}).(P_{12}-P_{21})}{||P_{22}-P_{21}||\,||P_{12}-P_{21}||}\right) \tag{5.2b}$$

$$\delta = arccos\left(\frac{(P_{21}-P_{11}).(P_{12}-P_{21})}{||P_{21}-P_{11}||\,||P_{12}-P_{21}||}\right) \tag{5.2c}$$

$$\alpha + \beta + \chi + \delta = 2\pi \tag{5.2d}$$

By solving similar sets of equations at each vertex in a fold-line, the crease pattern was generated for the parameters in Table 5.1. MATLAB function *vpasolve*() was used to solve these equations numerically [49].

5.2 Experimental Setup Details

In the experimental study by Arya and Pellegrino [48], the octagonal sheet generated using crease pattern described in Section 5.1 was perforated with a laser along fold-lines and 36 % of material along each fold-line was removed to fold easily. In the folded configuration, the hub was suspended in the middle with a string. The deployment was controlled by linear actuators that pulled the two tabs tangentially in two opposite directions. Deployment forces were recorded using the force sensors attached to the linear actuators. Deployment forces were plotted as a function of deployment coefficient (defined as the partially deployed diameter, D divided by the fully deployed diameter, D_f). Figure 5.2 shows the experimental setup used in the study.

Weight of the membrane was offloaded through the string supporting the hub and through the force sensors supporting the tabs to minimize the effect of gravity. Effect of air drag was reduced by ensuring quasi-static nature of deployment by maintaining a deployment rate (q) of 0.78 mm/s. However, the membrane could not be fully deployed as the membrane collapsed when the fold angles reached 180° (at a deployment coefficient of 0.9).

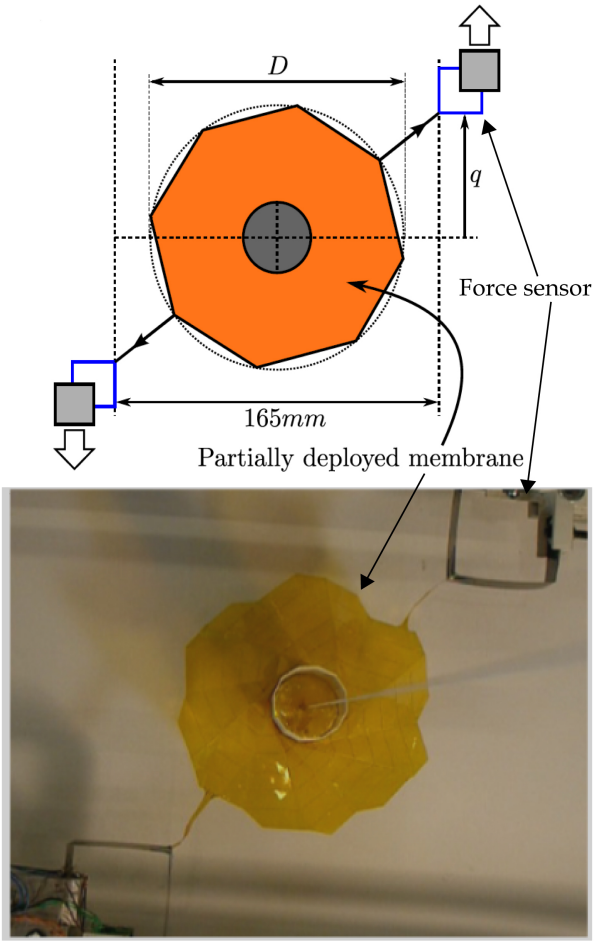

Figure 5.2: Experimental setup [48]

5.3 Solar Sail Finite Element Model

Numerical model of solar sail was setup in Abaqus/Explicit finite element package. To study the deployment behaviour, the intial folded configuration should be accurately captured. In these simulation, an ideal scenario of vertices of membrane panels in the folded state lying radially linear at each vertex of the hub was considered (see Figure 5.1(b)). The membrane panel geometry in the folded configuration (see Figure 5.4(a)) was created in AutoCAD and meshed in Abaqus/Explicit. Three-node reduced integrated shell elements, S3R were used to model the membrane panels. Crease lines were represented by two-node connector elements, CONN3D2 as described in Chapter 4. The hub was modeled as a rigid body. The finite element model of the membrane consisted of 19522 shell elements and 12642 nodes.

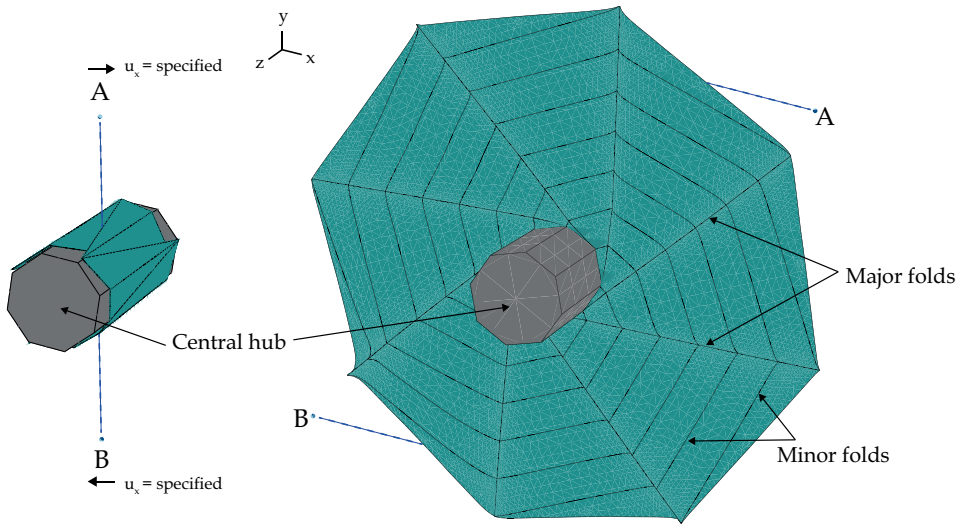

(a) Folded state (b) Deployed state

Figure 5.3: Finite element geometry of solar sail model

Simulation sequence was set to follow the experiment discussed in Section 5.2. Two reference nodes (A and B) were defined 165 mm apart to exert the pulling displacement of 150 mm in two opposite directions, (+)ve x and (-)ve x direction respectively. A *Link* connector element was used to attach the reference point to the membrane ensuring a constant distance in between during the simulation. Reaction force at node A was recorded throughout the simulation. All degrees of freedom of the hub were restrained except for rotation about z.

Material properties of Kapton were defined as given in Table 4.1. The definition of several contact surfaces is also required, as different parts of the solar sail will come into contact with each other and also with the rigid hub during deployment. The *General Contact* feature was assigned to the entire model by specifying *Contact Inclusions, All Exterior*. With this option Abaqus/Explicit automatically defines potential contact surfaces that will come into contact. *Hard* contact property that uses penalty stiffness was used.

There are two types of fold-lines in this particular model; major folds, which are aligned radially folded upto 180° at compacted state and minor folds, which are aligned circumferentially where the membrane is folded by 22.5° during compaction as illustrated in Figure 5.3. Rotational stiffness of minor folds was

assumed negligible as they are folded to a negligible angle during compaction. Rotational stiffness for major folds were assigned as discussed in Section 4.2. Rotational stiffness was reduced by 36 % to account for scoring as described in Section 5.2. Neutral angle was assumed to be zero as it was not recorded during experimental study.

5.4 Abaqus/Explicit Solver

Abaqus/Explicit solver was initially designed to solve dynamic high speed impact events. It implements central difference time integration rule with the use of diagonal or lumped element mass matrices, to solve for dynamic equilibrium where inertia plays a significant role given as follows.

$$m\ddot{u} = e - i \tag{5.3}$$

where m is the mass matrix, e is the external load vector and i is the internal load vector.

Recently, Explicit solver has been used to solve static problems by taking precautions to keep the term on the left hand side of Equation 5.3 negligible. In fact, explicit procedure has proven efficient in solving quasi static problems with complicated contact problems when compared to implicit solvers. In addition, when the models become very large and complex explicit procedure uses fewer resources than implicit procedure.

In this case, the deployment simulation of solar sail involves discontinuities such as dynamic snapping which is better handled by explicit than implicit solver. These phenomena will result in numerical instabilities and the convergence will be affected by singularity in stiffness matrix. To avoid stiffness matrix in computation, explicit procedure which advances the kinematic state of each degree of freedom by direct integration of its equations of motion has been adopted. However, effort should be made to simulate the deployment event in the shortest time, keeping the effects of inertia insignificant.

5.4.1 Energy balance in quasi-static analysis

In order to confirm that the effects of inertia are insignificant, at any particular time, kinetic energy in the system should be a very small percentage of internal energy, generally lesser than 1% to 5% of internal energy [18].

Further, the robustness of a particular analysis can be verified by investigating the energy history. Mainly the total energy in the system, E_{total} should be equal to the total energy introduced to the system externally. According to Abaqus/Explicit terms for the deployment simulation of a solar sail, energy balance equation can be written as follows.

$$E_{total} = E_i + E_{vd} + E_{ke} - E_{wk} \tag{5.4}$$

where E_i is the internal energy which is the summation of elastic, inelastic strain energy and artificial energy, E_{vd} is the viscous dissipation, E_{ke} is the kinetic energy and E_{wk} is the work done by the external forces.

If the energy balance shows any discrepancy, the solution has not converged properly, in this case necessary measures should be taken to maintain the quasi-static state and ensure the analysis is free from any numerical instabilities. Artificial energy should be a very small percentage of internal energy, generally lesser than 1% to 2% of internal energy [18] as well to ensure that the simulation free from artificial effects like hour glassing, shear locking etc. Therefore, during an explicit simulation, it is essential to check the energy history before coming to a conclusion from the output.

5.4.2 Economising the solution

While solving in explicit procedure, out of balance forces are propagated as stress waves to adjacent elements. In order to capture these stress waves, the stable time increment should be small enough. Explicit time integration is stable only if the time increment is lesser than the time for a wave to travel between adjacent nodes in the finite element mesh which is known as the Courant condition [50]. Therefore, central difference operator is conditionally stable, and when the system

includes damping to control high frequency oscillations, the stability limit for the operator is given in terms of the highest eigenvalue in the system as given below.

$$\Delta t \leqslant \frac{2}{\omega_{max}} \left(\sqrt{1 - \xi^2} - \xi \right) \tag{5.5}$$

This condition can be considered as an approximate equation for minimum stable time increment as follows.

$$\Delta t = \alpha \left(\sqrt{1 - \xi^2} - \xi \right) \frac{l_{min}}{c_d} \tag{5.6}$$

where α, ξ, l_{min} and c_d denote time scaling factor, fraction of critical damping in the fundamental frequency mode, the shortest length of finite element and the dilatational wave speed, respectively. Dilatational wave speed can be expressed as follows.

$$c_d \approx \sqrt{\frac{\mathrm{E}}{\rho}} \tag{5.7}$$

where E and ρ denote modulus of elasticity and material density, respectively.

This shows that the size of the time increment is purely dependent on the highest natural frequency of the model, material properties and element size, despite the type of loading. Therefore, it is impractical to model the process in its natural time period. For example, initial estimated stable time increment for the model created as per Section 5.3 was 1 x 10^{-7} s. To deploy to 150 mm at a deployment rate of 0.78 mm/s as in the experimental study, it will take approximately 193 s. Thereby it will require 1.93 x 10^9 increments if the loading rate is to be maintained as per the experiment, which is very costly. Hence, artificially increasing the speed of the process is necessary to achieve economic solution. This can be achieved through three methods, viz; *increasing loading rate*, *applying viscous pressure* and *mass scaling*.

Loading rate

In this method, the time scale of the process is artificially reduced by increasing the loading rate. Hence, a fewer no of increments is enough to solve the process compared to solving in its natural time period. However, high loading rate will emphasize the dynamic responses. Hence, it is essential to strike a balance. Abaqus [18] recommends to use a time scale of 10 times the fundamental natural period of the structure as an initial estimate. For the solar sail model described in Section 5.3, fundamental natural period was computed by doing a frequency analysis in Abaqus/Standard. The estimated period was 0.091 s, hence the definition of the overall loading rate was initially set such that deployment would occur over a time period of ten times the fundamental period, or 0.91 s. However, the kinetic energy was beyond the limit of 1% to 5% of internal energy for this time scale. By trial and error process, a time scale of 3 s was chosen finally, where the kinetic energy can be maintained within the limits.

The concern while applying load/displacement is, it should not create any significant inertial effects in the structure which violate the quasi-static condition. Hence, the load/displacement should be applied as smooth as possible. In the simulation, the displacement of the reference points were applied through a fifth order polynomial function of time with first and second time derivatives equal to zero at the beginning and end of the time interval using the Abaqus/Explicit command **Amplitude, Definition = Smooth Step*. This ensures the smoothness of the displacement application, so as to not cause any accelerations imposed on the structure at the beginning and the end of a particular action.

Viscous pressure

Viscous pressure loading is an effective way to damp out dynamic effects quickly, and thus reach quasi-static equilibrium in a minimal number of increments. A viscous pressure load generates a normal velocity-dependent pressure on surfaces. This pressure can be written in the form of,

$$p = -c_v v.n \tag{5.8}$$

where c_v is the damping coefficient, v is the velocity and n is the normal vector.

Since this is applied as an external load, this damping will not directly affect the stable time increment given in Equation 5.6. However, if the value of c_v is high, it will over damp the structure and produce erroneous results. Typically, initial guess for c_v is chosen as a very small percentage (below 2%) of ρc_d, given as follows.

$$\rho c_d = \rho \sqrt{\frac{\mathrm{E}(1-\nu)}{\rho(1+\nu)(1-2\nu)}} \tag{5.9}$$

where ρ, E, ν denotes material density, modulus of elasticity and Poisson's ratio respectively.

The value of ρc_d is approximately equal to 2 x 10^{-3} for the current simulation. Hence, initially a value of 4 x 10^{-5} was chosen for c_v (2% of ρc_d). However, this caused high deformation in the elements during the simulation. By a trial and error process, a value of 4 x 10^{-8} was chosen finally, just enough for the simulation to complete.

Mass scaling

Increasing the mass of a structure results in the decrease in dilatational wave speed, c_d (Equation 5.7) of the structure, thus increasing the stable time increment, Δt (Equation 5.6). However, increasing the mass will increase the inertial effects. Hence, it is necessary to strike a balance. Artificially increasing the material density by a factor of f^2 increases the stable time increment by a factor of f.

In this simulation, **FIXED MASS SCALING, TYPE=BELOW MIN, DT=dt* command in Abaqus/Explicit was used to scale only elements whose stable time increment is below the value assigned to DT so that their stable time increment equals dt. In order to select a suitable value for dt, a sensitivity analysis was carried out. Figure 5.4 shows a comparison of kinetic energy of the structure for simulations carried out for two different values of dt with typical internal energy. Based on the results dt = 1 x 10^{-6} was chosen where the kinetic energy was within the acceptable limits as discussed in Section 5.4.1. The sudden spikes in the kinetic energy at certain locations in the plots indicate dynamic snapping

effect discussed earlier in Section 1.3 which the simulation has captured.

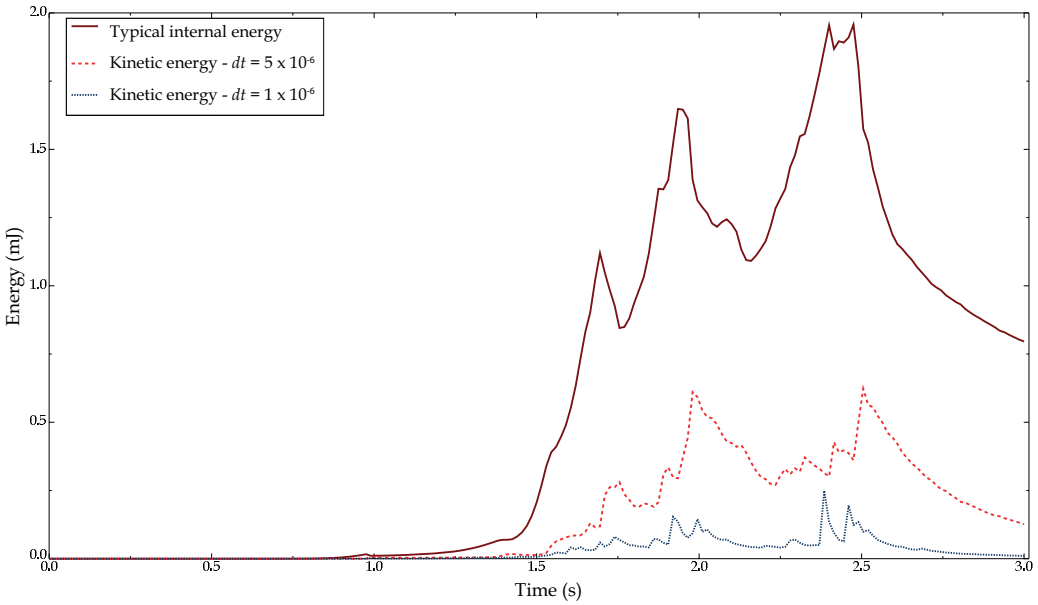

Figure 5.4: Comparison of kinetic energy profiles for different mass scaling

5.5 Results and Discussion

Figure 5.5 shows energy balance checks carried out to identify any numerical instabilities in the simulation as discussed in Section 5.4.1. The initial simulation yielded a high viscous dissipation energy compared to internal energy which is an indication of external factors influencing the results. This was due to the default contact damping force (f_{vd}) for penalty contact applied in Abaqus/Explicit which is expressed as follows.

$$f_{vd} = \mu_0 A v_{rel}^{el} \tag{5.10}$$

where A is the nodal area, v_{rel}^{el} is the rate of relative motion between the two surfaces and μ_0 is the damping coefficient. By default, μ_0 is set to 0.03 Ns/m. This resulted in the high viscous dissipation. This was overridden with the command **CONTACT DAMPING, DEFINITION=DAMPING COEFFICIENT, 0*, setting μ_0 to 0. This yielded a negligible viscous dissipation energy as shown in the figure. However, it was observed that the total energy experienced an increase towards the end for this simulation. This is an

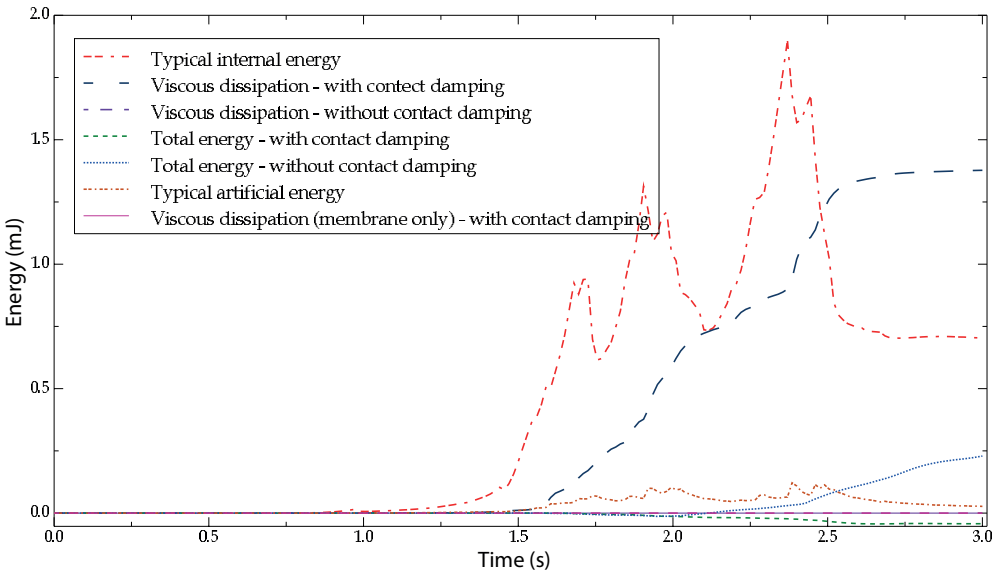

Figure 5.5: Energy variation with contact damping

indication of numerical instabilities. Hence it was decided not to set μ_0 to 0.

Further investigation of viscous dissipation energy of the membrane alone for $\mu_0 = 0.03$ Ns/m showed that it is negligible. This confirms that the membrane is unaffected by the viscous damping under question. As we are only interested in the deployment forces of the membrane, it is acceptable to follow the results thus obtained. It should be noted that the total energy for this simulation is close to zero throughout the simulation, confirming that the simulation is free from numerical instabilities. However, artificial energy lies in 5% to 10% range of internal energy. Abaqus inputs artificial energy during contact and when elements distort to ensure numerical errors do not disrupt the energy balance. This requires further investigation.

Figure 5.6 shows deployment force recorded at node A plotted against deployment coefficient, D/D_f as described in Section 5.2. D was recorded in the simulations as the distance between the two points in the membrane that are attached to link connectors. MATLAB function smooth (x, y, span, 'rloess') was used to reduce the noise of raw data where the span was set to 0.1. The 'rloess' method is a local regression analysis that uses weighted linear least squares and a 2nd degree polynomial model and assigns lower weight to outliers in the regression. For comparison, deployment force for model that has

fold-lines without rotational stiffness is also plotted.

The general trend of deployment force observed in the experiment is of two phases. The first phase is upto 80% deployment with almost zero stiffness and the second phase is with increasing stiffness. Initial hypothesis for this increasing stiffness is that it is due to increasing stiffness of fold-lines. However, both simulations with and without fold-line stiffness exhibit this behaviour. Therefore, this might be due to stretching of the membrane panels. Membrane stresses were not recorded during the experiment. This requires further investigation.

However, the deployment with fold-line stiffness was smoother compared to deployment without fold-lines. The deployment without fold-line stiffness exhibits sudden spikes in deployment force. This might be due to dynamic snapping effect. This created overshooting in the model without fold-line stiffness, but the model with fold-line stiffness could resist that by the stiffness provided by fold-lines with only minor fluctuations. Figure 5.7 shows snapshots taken during deployment simulation at different deployment coefficients for both models. At the deployment coefficient of 0.39, the overshooting is clearly visible in the model without fold-line stiffness, which was not observed in the model with fold-line stiffness.

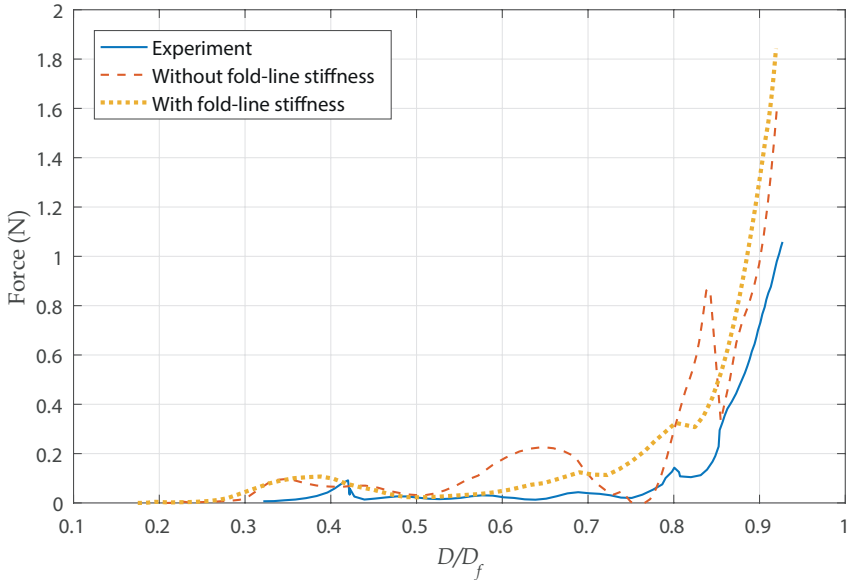

Figure 5.6: Deployment force

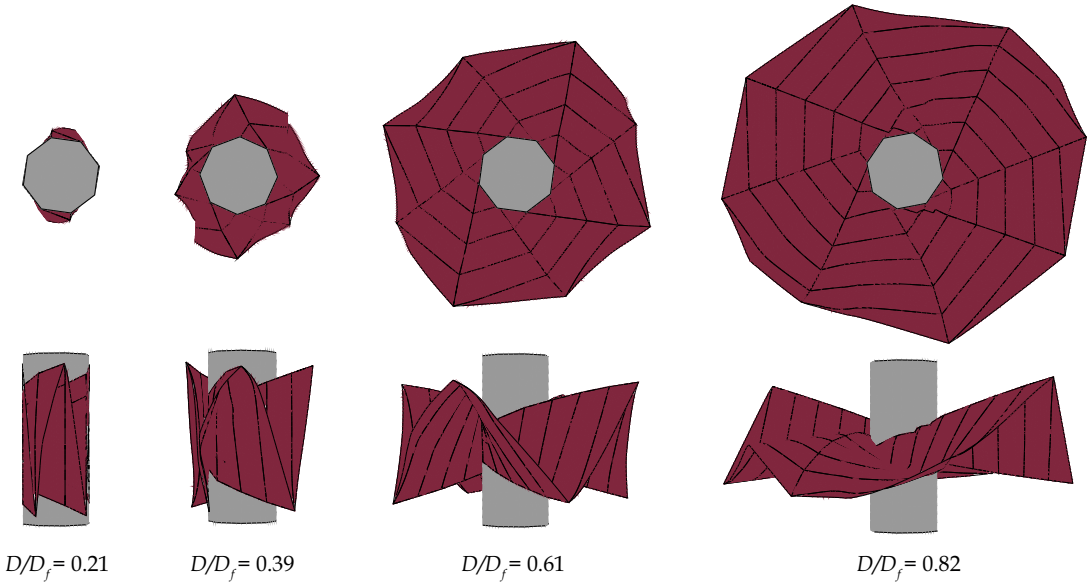

(a) without fold-line stiffness

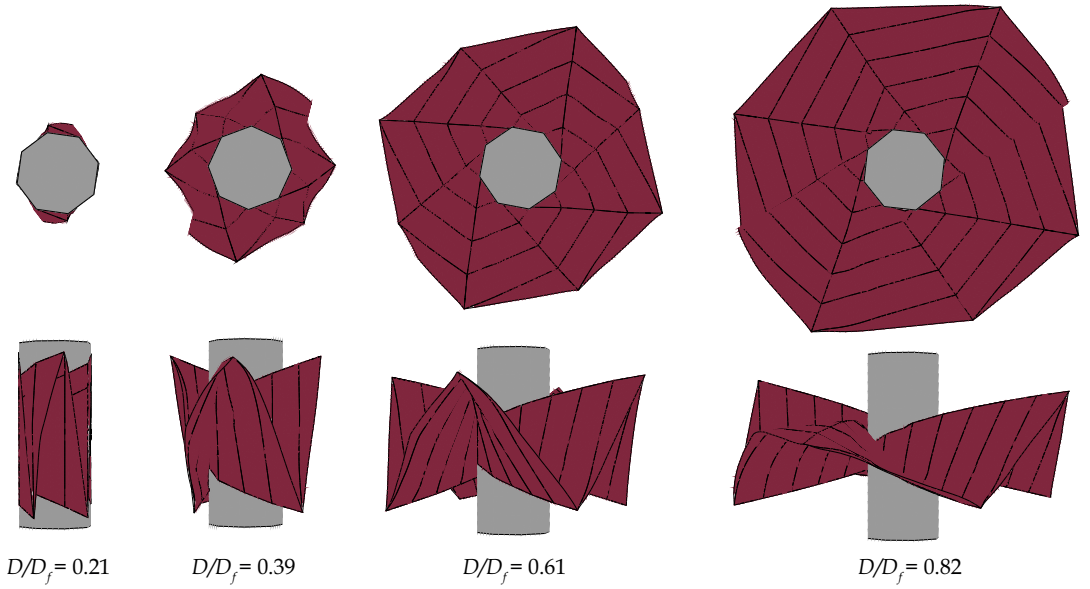

(b) with fold-line stiffness

Figure 5.7: Plan and isometric snapshots during deployment simulation at different deployment coefficients

Chapter 6

Conclusions and Future Work

6.1 Conclusions

Fold-lines create permanent plastic deformation in thin membranes which alter their physical state and behaviour. It has been emphasized in the past studies that the effect of fold-lines is captured in virtual tests that are aimed at studying the folded membrane structures. This thesis presents a simulation technique that can be used to carry out virtual tensile tests on single-folded thin membranes to quantify their moment-rotation response, which is one of the key properties of fold-lines.

The comparison of fold-line stiffness determined from the proposed virtual testing of Kapton membranes, with the experimental data as per available literature shows that the values are in the same order. The deviations in exact values could be owing to the experimental difficulties involved in the measurement of angles using digital imaging, and the adopted creasing and loading procedure without adequate calibration.

A further comparison was made with results from Elastica theory. A reasonable agreement is achieved between the moment rotation response from simulating 25 μm Kapton membrane (creased to a creasing gauge of 2 times the thickness of membrane) and the solution obtained from Elastica, for tensile loading above 0.02 N. However, the inherent assumptions and the absence of simple solving techniques limit the possibility of quantifying fold-line mechanics using Elastica theory. It is evident that the finite element analysis techniques prove to be substantially competent for the simulation of creased geometry and conducting numerical tensile tests on single folded thin membranes.

A strategy for implementing the fold-line stiffness thus obtained in

commerical finite element packages is also presented. The proposed fold-line idealisation scheme is to represent fold-lines with connectors defined with rotational stiffness. For demonstration, unfolding of a single folded Kapton membrane to an external tensile load is simulated using commercial finite element package Abaqus/Standard and validated against physical experiments. The proposed technique with connector elements is meritorious over other available techniques as it captures both the deformed profile and axial displacements along the folded membrane with close agreement with experimental results.

The proposed strategy with the fold-line stiffness determined from virtual testing was used to study the quasi-static deployment behaviour of a solar sail model with 25 μm thick membrane wrapped around a polygonal hub using Abaqus/Explicit package. However, the fold-line stiffness had little effect on the deployment force of the sail in the range of deployment carried out experimentally. It is to be noted that the simulation was based on several assumptions, namely; neutral angles of all fold-lines are zero, the fold-line stiffness is uniform along the length of the fold-line and the effect of scoring can be captured by reducing fold-line stiffness.

6.2 Future Work

The following are some suggested future research directions.

1. Developing a framework for quantifying fold-line stiffness of thin folded membranes at a wider load regime.

2. Quantifying the behaviour of asymmetric fold-lines and interacting fold-lines at a vertex of a folded membrane.

3. Carrying out experimental studies to verify the effect of fold-line stiffness at higher deployment coefficients while recording membrane stresses through Digital Image Correlation techniques (DIC) and validating with numerical studies as suggested.

References

[1] R. W. Ridenoure, R. Munakata, S. D. Wong, A. Diaz, D. A. Spencer, D. A. Stetson, B. Betts, B. A. Plante, J. D. Foley, and J. M. Bellardo, "Testing The LightSail Program: Advancing Solar Sailing Technology Using a CubeSat Platform," *Journal of Small Satellites*, vol. 5, no. 2, pp. 531–550, 2016. 1

[2] C. Liu and Y. Shi, "Comprehensive structural analysis and optimization of the electrostatic forming membrane reflector deployable antenna," *Aerospace Science and Technology*, vol. 53, pp. 267–279, 2016. 1

[3] NASA, "Thin-Films with Integrated Structural and Functional Elements," 2015. [Online]. Available: https://technology.nasa.gov/patent/LAR-TOPS-203 1

[4] C. Sickinger and E. Breitbach, "Ultra-Lightweight Deployable Space Structures," in *4th International Conference on Thin-Walled Structures*, Loughborough, England, 2004. 1

[5] V. Lappas, N. Adeli, L. Visagie, J. Fernandez, T. Theodorou, W. Steyn, and M. Perren, "CubeSail: A low cost CubeSat based solar sail demonstration mission," *Advances in Space Research*, vol. 48, no. 11, pp. 1890–1901, 2011. 1

[6] D. Lichodziejewski, B. Derbès, K. Slade, and T. Mann, "Vacuum deployment and testing of a 4-quadrant scalable inflatable rigidizable solar sail system," in *46th AIAA/ASME/ASCE/AHS/ASC Structures, Structural Dynamics, and Materials Conference*, Austin, Texas, 2005. 2

[7] H. Furuya, Y. Inoue, and T. Masuoka, "Deployment characteristics of rotationally skew fold membrane for spinning solar sail," in *46th*

AIAA/ASME/ASCE/AHS Structures, Structural Dynamics, and Materials Conference, Austin, Texas, 2005. 2

[8] U. Geppert, B. Biering, F. Lura, J. Block, M. Straubel, and R. Reinhard, "The 3-step DLR-ESA Gossamer road to solar sailing," *Advances in Space Research*, vol. 48, no. 11, pp. 1695–1701, 2011. 2

[9] C. Katan, "Nasa's next solar sail: lessons learned from nanosail-d2," in *26th Annual AIAA/USU Conference on Small Satellites: Enhancing Global Awareness through Small Satellites*, 2012. 3

[10] B. B. Betts, B. Nye, J. Vaughn, E. Greeson, R. Chute, D. A. Spencer, R. W. Ridenoure, R. Munakata, S. D. Wong, A. Diaz, D. A. Stetson, J. D. Foley, J. M. Bellardo, and B. A. Plante, "LightSail 1 Mission Results and Public Outreach Strategies," in *Fourth International Symposium on Solar Sailing*, Kyoto, Japan, 2017. 3

[11] B. B. Betts, D. A. Spencer, B. Nye, R. Munakata, J. M. Bellardo, S. D. Wong, A. Diaz, R. W. Ridenoure, B. A. Plante, J. D. Foley, and J. Vaughn, "LightSail 2 : Controlled Solar Sailing Using a CubeSat," in *Fourth International Symposium on Solar Sailing*, Kyoto, Japan, 2017. 3

[12] E. T. Filipov, K. Liu, T. Tachi, M. Schenk, and G. H. Paulino, "Bar and hinge models for scalable analysis of origami," *International Journal of Solids and Structures*, vol. 124, pp. 26–45, 2017. 4

[13] R. Funase, M. Sugita, O. Mori, Y. Tsuda, and J. Kawaguchi, "Modeling of Spinning Solar Sail By Multi Particle Model and Its Application To Attitude Control System," in *Proceedings of the ASME 2009 International Design Engineering Technical Conferences & Computers and Information in Engineering Conference*, San Diego, California, 2009. 4

[14] H. Sakamoto, M. C. Natori, S. Kadonishi, Y. Satou, Y. Shirasawa, N. Okuizumi, O. Mori, H. Furuya, and M. Okuma, "Folding patterns of planar gossamer space structures consisting of membranes and booms," *Acta Astronautica*, vol. 94, pp. 34–41, 2014. 5

[15] J. Cai, Z. Ren, Y. Ding, X. Deng, Y. Xu, and J. Feng, "Deployment simulation of foldable origami membrane structures," *Aerospace Science and Technology*, vol. 67, no. April, pp. 343–353, 2017. 5, 6, 32, 34, 37

[16] B. Y. Dharmadasa, "Simulation of Fold-Line Stiffness in Deployable Membranes," Master's thesis, University of Moratuwa, 2017. 5, 6, 14, 37

[17] Dupont, "DEC Kapton summary of properties," 2015. [Online]. Available: http://www.dupont.com/products-and-services/membranes-films/polyimide-films/brands/kapton-polyimide-film/products/kapton-fn.html 5, 22, 23

[18] Abaqus, "Analysis User's Guide," Dassault Systemes Simulia Corp., Providence, Rhode Island, 2014. 5, 20, 45, 47

[19] B. Y. Dharmadasa, H. M. Y. C. Mallikarachchi, and F. Lopez Jimenez, "Characterizing the Mechanics of Fold-lines in Thin Kapton Membranes," in *2018 AIAA Spacecraft Structures Conference*. Kissimmee, Florida: American Institute of Aeronautics and Astronautics, 2018. 5, 15, 16, 17, 18, 20, 21, 23, 27, 37

[20] N. Hossain, K. Woo, and C. Jenkins, "Nonlinear Material Response of Systematically Creased Membranes," in *47th AIAA/ASME/ASCE/AHS/ASC Structures, Structural Dynamics, and Materials Conference*, Newport, Rhode Island, 2006. 6, 11, 29, 32, 33, 34, 36, 37

[21] S. D. Guest, "Deployable Structures : Concepts and Analysis," Ph.D. dissertation, 1994. 6, 8, 9, 39, 40

[22] K. Miura, "Method of packaging and deployment of large membranes in space," The Institute of Space and Astronautical Science, Tech. Rep., 1985. 7

[23] M. Schenk, "Folded Shell Structures," Ph.D. dissertation, University of Cambridge, 2011. 8, 9

[24] E. T. Filipov, T. Tachi, and G. H. Paulino, "Origami tubes assembled into stiff, yet reconfigurable structures and metamaterials," vol. 112, no. 40, pp. 12 321–12 326, 2015. 8, 10

[25] R. D. Resch, "The topological design of sculptural and architectural systems," in *Proceedings of the June 4-8, 1973, national computer conference and exposition on - AFIPS '73*. New York, USA: ACM Press, p. 643. 8, 9

[26] K. Kuribayashi, K. Tsuchiya, Z. You, D. Tomus, M. Umemoto, T. Ito, and M. Sasaki, "Self-deployable origami stent grafts as a biomedical application of Ni-rich TiNi shape memory alloy foil," *Materials Science and Engineering: A*, vol. 419, no. 1-2, pp. 131–137, mar 2006. 8, 9, 10

[27] C. Lv, D. Krishnaraju, G. Konjevod, H. Yu, and H. Jiang, "Origami based mechanical metamaterials," *Scientific Reports*, vol. 4, no. 1, p. 5979, may 2014. 8

[28] S. Felton, M. Tolley, E. Demaine, D. Rus, and R. Wood, "A method for building self-folding machines," *Science*, vol. 345, no. 6197, pp. 644–646, 2014. 10

[29] R. Hoffman, A. Pickett, D. Ulrich, E. Haug, D. Lasry, and J. Clinkemaillie, "A Finite Element Approach to Occupant Simulation: The PAM-CRASH Airbag Model," *SAE Technical Paper 890754*, 1989. 8

[30] NASA, "NASA's New Shape-Shifting Radiator Inspired by Origami," 2017. [Online]. Available: https://www.nasa.gov/feature/goddard/2017/nasa-s-new-shape-shifting-radiator-inspired-by-origami 8

[31] T. Tachi, "Designing freeform origami tessellations by generalizing reschs patterns," *Journal of Mechanical Design*, vol. 135 (11), pp. 111 006–111 006–10, 2013. 10

[32] J. L. Silverberg, J.-H. Na, A. A. Evans, B. Liu, T. C. Hull, C. D. Santangelo, R. J. Lang, R. C. Hayward, and I. Cohen, "Origami structures with a critical transition to bistability arising from hidden degrees of freedom," *Nature Materials*, vol. 14 (4), pp. 389–393, 2015. 10

[33] D. Dureisseix, "An overview of mechanisms and patterns with origami," *International Journal of Space Structures*, vol. 27 (1), pp. 1–14, 2012. 10

[34] A. L. Adler, "Finite element approaches for static and dynamic analysis of partially wrinkled membrane structures," Ph.D. dissertation, University of Colorado, 2000. 10

[35] A. Gough, N. M. A. Hossain, C. H. Jenkins, J. Blandino, and A. Hendricks, "Experimental and numerical study of creased membranes," in *46th AIAA/ASME/ASCE/AHS/ASC Structures, Structural Dynamics and Materials Conference*, Austin, TX, United States, 2005. 11

[36] B. Thiria and M. Adda-Bedia, "Relaxation mechanisms in the unfolding of thin sheets," *Phys. Rev. Lett.*, vol. 107 (2), p. 025506, Jul 2011. 11, 12

[37] F. Lechenault, B. Thiria, and M. Adda-Bedia, "Mechanical response of a creased sheet," *Phys. Rev. Lett.*, vol. 112 (24), p. 244301, Jun 2014. 11, 13, 17, 35

[38] R. MacNeal and W. Robbins, "Tensile properties of a tape with a transverse crease," Astro Research Corporation, Tech. Rep., 1966. 12

[39] D. Murphy, T. Trautt, M. McEachen, D. Messner, G. Laue, and P. Gierow, "Progress and plans for system demonstration of a scalable square solar sail," in *14th AAS/AIAA Space Flight Mechanics Conference*, AAS, San Diego, CA, 2004. 12

[40] K. Woo, K. Nandukar, and C. H. Jenkins, "Effective modulus of creased thin membranes," *Journal of Spacecraft and Rockets*, vol. 45 (1), pp. 19–26, 2008. 12

[41] D. Sleight, Y. Michii, D. Lichodziejewski, B. Derbes, T. Mann, K. Slade, and J. Wang, "Finite Element Analysis and Test Correlation of a 10-Meter Inflation-Deployed Solar Sail," in *46th AIAA/ASME/ASCE/AHS/ASC Structures, Structural Dynamics and Materials Conference*, Austin, Texas, 2005. 14

[42] M. Liyanage and H. M. Y. C. Mallikarachchi, "Origami based folding patterns for compact deployable structures," in *4th International Conference for Structural Engineering and Construction Management*, Kandy, Sri Lanka, December 2013. 14

[43] N. Okuizumi and T. Yamamoto, "Centrifugal Deployment of Membrane with Spiral Folding: Experiment and Simulation," *Journal of Space Engineering*, no. 1, pp. 41–50, 2009. 14

[44] A. Papa and S. Pellegrino, "Systematically Creased Thin-Film Membrane Structures," *Journal of Spacecraft and Rockets*, vol. 45, no. 1, pp. 10–18, jan 2008. 14, 16

[45] A. C. Andrew, B. C. Philip, J. J. James, R. W. Gregory, and V. A. Richard, "Characterization of creases in polymers for adaptive origami structures,"

in *ASME 2014 Conference on Smart Materials, Adaptive Structures and Intelligent Systems SMASIS2014*, Newport, Rhode Island, 2014. 16, 29

[46] S. Mierunalan and H. M. Y. C. Mallikarachchi, "Prediction of creased geometry of thin folded membranes using finite element analysis," in *3rd International Moratuwa Engineering Research Conference, MERCon 2017*, Colombo, Sri Lanka, 2017, pp. 283–287. 16, 21

[47] C. Pradier, J. Cavoret, D. Dureisseix, C. Jean-Mistral, and F. Ville, "An Experimental Study and Model Determination of the Mechanical Stiffness of Paper Folds," *Journal of Mechanical Design*, vol. 138, no. 4, p. 041401, 2016. 16, 17

[48] M. Arya and S. Pellegrino, "Deployment mechanics of highly compacted thin membrane structures," in *Spacecraft Structures Conference*, National Harbor, Maryland, 2014, pp. 1–14. 39, 41, 42

[49] Mathworks, "Solve equations numerically - MATLAB vpasolve," 2018. [Online]. Available: https://www.mathworks.com/help/symbolic/vpasolve.html 41

[50] T. Belytschko, W. K. W. K. Liu, B. B. Moran, and K. I. Elkhodary, *Nonlinear finite elements for continua and structures*. John Wiley & Sons, 2014. 45

Appendix

Keywords of Abaqus Input Files

1. Predicting Mechanical Properties of Fold-Lines

```
**----------------------------------------
** MATERIAL PROPERTY DEFINITION
**----------------------------------------
*Material, name=Kapton
*Density
1.42e-09,
*Elastic
2500., 0.34
*Plastic
69., 0.
78.654, 0.0045384
87.183, 0.0111268
93.902, 0.0184392
101.397, 0.0254412
107.083, 0.0331668
112.51, 0.040996
117.42, 0.049032
..... .....
224.931, 0.586028
226.224, 0.59551
227.516, 0.604994
228.808, 0.614477
230.1, 0.62396
230.1, 1.
```

2. Deployment Simulation of Single-Folded Membrane

```
**----------------------------------------
** CONSTRAINT DEFINITION
**----------------------------------------
* Constraint: tie
*Tie, name=tie, adjust=yes, no rotation,
type=NODE TO SURFACE
**----------------------------------------
** CONNECTOR PROPERTY DEFINITION
**----------------------------------------
Connector Behavior, name=elastic
*Connector Elasticity, component=4
0.018,
**----------------------------------------
** MATERIAL PROPERTY DEFINITION
**----------------------------------------
*Material, name=Kapton-lin
*Density
1.42e-09,
*Elastic
2500., 0.34
**
```

3. Quasi-static Deployment of a Solar Sail

```
**----------------------------------------
** CONSTRAINT DEFINITION
**----------------------------------------
** Constraint: tie
*Tie, name=tie, adjust=yes, no rotation,
type=SURFACE TO SURFACE
**----------------------------------------
** CONNECTOR PROPERTY DEFINITION
```

```
**----------------------------------------------------------
*Connector Behavior, name=elastic
*Connector Elasticity, component=4
0.018,
**----------------------------------------------------------
** ELEMENT CONTROL
**----------------------------------------------------------
*Section Controls, name=EC-1
1., 1., 1., 0.01, 1.
*Amplitude, name=Smooth, definition=SMOOTH STEP
0., 0., 4.1, 1.
**----------------------------------------------------------
** MATERIAL PROPERTY DEFINITION
**----------------------------------------------------------
*Material, name=Hub
*Density
1.42e-09,
*Elastic
200000., 0.3
*Material, name=Kapton
*Density
1.42e-09,
*Elastic
2500., 0.34
**----------------------------------------------------------
** INTERACTION PROPERTY
**----------------------------------------------------------
*Surface Interaction, name=contactproperty
*Surface Behavior, pressure-overclosure=HARD
**----------------------------------------------------------
** BOUNDARY CONDITIONS
**----------------------------------------------------------
** Name: Hub Type: Displacement/Rotation
*Boundary
Set-5, 1, 1
Set-5, 2, 2
Set-5, 3, 3
```

```
Set-5, 4, 4
Set-5, 5, 5
**----------------------------------------------------------------
** INTERACTIONS
**----------------------------------------------------------------
** Interaction: Contact
*Contact, op=NEW
*Contact Inclusions, ALL EXTERIOR
*Contact Property Assignment,contactproperty
**----------------------------------------------------------------
** STEP: Deploy
**----------------------------------------------------------------
*Step, name=Deploy, nlgeom=YES
*Dynamic, Explicit
, 4.2
*Bulk Viscosity
0., 0.
** Mass Scaling: Semi-Automatic
** Whole Model
*Fixed Mass Scaling, dt=1e-06, type=below min
**----------------------------------------------------------------
** BOUNDARY CONDITIONS
**----------------------------------------------------------------
** Name: RP1 Type: Displacement/Rotation
*Boundary, amplitude=Smooth
RP1, 1, 1, 140.
RP1, 2, 2
** Name: RP2 Type: Displacement/Rotation
*Boundary, amplitude=Smooth
RP2, 1, 1, -140.
RP2, 2, 2
**----------------------------------------------------------------
** LOADS
**----------------------------------------------------------------
** Name: viscous Type: Pressure
*Dsload, ref node=Set-26
Surf-129, VP, 2e-08
```